the plant journal

SEB SOCIETY FOR EXPERIMENTAL BIOLOGY

The Plant Journal (2020) **103,** 1399–1419 doi: 10.1111/tpj.14808

Exocyst mutants suppress pollen tube growth and cell wall structural defects of *hydroxyproline O-arabinosyltransferase* mutants

Steven Beuder[1], Alexandria Dorchak[1], Ashwini Bhide[1], Svenning Rune Moeller[2], Bent L. Petersen[2] and Cora A. MacAlister[1]*

[1]*Department of Molecular, Cellular and Developmental Biology, University of Michigan, 1105 N. University Ave, Ann Arbor, MI, 48109, USA, and*

[2]*Department of Plant and Environmental Sciences, Faculty of Science, University of Copenhagen, Thorvaldsensvej 40, København1871 Frederiksberg C, Denmark*

Received 20 February 2020; revised 22 April 2020; accepted 28 April 2020; published online 11 May 2020.
*For correspondence (e-mail macalist@umich.edu).

SUMMARY

HYDROXYPROLINE *O*-ARABINOSYLTRANSFERASEs (HPATs) initiate a post-translational protein modification (Hyp-Ara) found abundantly on cell wall structural proteins. In *Arabidopsis thaliana*, *HPAT1* and *HPAT3* are redundantly required for full pollen fertility. In addition to the lack of Hyp-Ara in *hpat1/3* pollen tubes (PTs), we also found broadly disrupted cell wall polymer distributions, particularly the conversion of the tip cell wall to a more shaft-like state. Mutant PTs were slow growing and prone to rupture and morphological irregularities. In a forward mutagenesis screen for suppressors of the *hpat1/3* low seed-set phenotype, we identified a missense mutation in *exo70a2*, a predicted member of the vesicle-tethering exocyst complex. The suppressed pollen had increased fertility, fewer morphological defects and partially rescued cell wall organization. A transcriptional null allele of *exo70a2* also suppressed the *hpat1/3* fertility phenotype, as did mutants of core exocyst complex member *sec15a*, indicating that reduced exocyst function bypassed the PT requirement for Hyp-Ara. In a wild-type background, *exo70a2* reduced male transmission efficiency, lowered pollen germination frequency and slowed PT elongation. EXO70A2 also localized to the PT tip plasma membrane, consistent with a role in exocyst-mediated secretion. To monitor the trafficking of Hyp-Ara modified proteins, we generated an HPAT-targeted fluorescent secretion reporter. Reporter secretion was partially dependent on *EXO70A2* and was significantly increased in *hpat1/3* PTs compared with the wild type, but was reduced in the suppressed *exo70a2 hpat1/3* tubes.

Keywords: secretion, pollen tube, cell wall, glycoprotein, tip growth, exocyst, *Arabidopsis thaliana*.

INTRODUCTION

For plant cells to grow, the cell wall must be sufficiently extensible to accommodate cell expansion while maintaining enough strength to prevent cell rupture from the high turgor pressure of the cytoplasm. This balance is especially critical to tip-growing cell types, like pollen tubes (PTs) and root hairs, where expansion happens at a single growing point. With their inherent growth polarity, tip-growing cells may be divided into two general cell wall domains, an extensible tip and a rigid shaft. Cell wall properties depend on the polymer composition, and the tip and shaft region differ in functionally significant ways (Bosch and Hepler, 2005; Dardelle *et al.*, 2010; Rounds *et al.*, 2011; Chebli *et al.*, 2012; Hepler *et al.*, 2013). PTs are generally rich in pectic polysaccharides, which are initially secreted in a methyl-esterified form. The methyl-esterified pectins are de-esterified in the wall by pectin methylesterases (PMEs), after which they are able to form a gel through divalent ion cross-linking, contributing to cell wall rigidity (Bosch and Hepler, 2005; Wolf *et al.*, 2009). In PTs, the shaft is further reinforced by the deposition of callose (1,3-β-D-glucan) (Schlupmann *et al.*, 1994; Van der Woude *et al.*, 1971). In contrast to other plant cell types, PTs contain relatively little cellulose (1,4-β-D-glucan). Although cellulose and callose are synthesized at the plasma membrane, other wall polymers are synthesized by the endoplasmic reticulum (ER) and Golgi-resident enzymes, and must be delivered, along with other secretory cargos, by secretory vesicles, although much is unknown about the process (Cosgrove, 2005; Sinclair *et al.*, 2018).

To support the rapid growth of PTs, secretion must also be very rapid in these cells (Campanoni and Blatt, 2007). Cell expansion and cell wall accumulation are temporally related, with secretion leading to thickening of the wall followed by an increase in the growth rate during oscillatory PT growth (McKenna *et al.*, 2009). The vesicle dynamics at the tip of the PT are complex and include a mix of exocytic vesicle movement, plasma membrane fusion and endocytic recycling of excess membrane (Bove *et al.*, 2008). Multiple components of the PT secretory pathway have been described, including several members of the vesicle-tethering exocyst protein complex. The exocyst is an octomeric complex composed of one of each of its subunits (SEC3, SEC5 SEC6, SEC8, SEC10, SEC15, EXO70 and EXO84). The exocyst is well conserved across the Eukaryota (Mei and Guo, 2018), and in plants, exocyst complex members have been implicated in several important biological processes, including casparian strip formation (Kalmbach *et al.*, 2017), compatible pollen reception by the stigma (Samuel *et al.*, 2009; Safavian *et al.*, 2015), tracheary element development (Li *et al.*, 2013), polar organ growth, root hair elongation (Synek *et al.*, 2006), root growth (Cole *et al.*, 2014), and pollen germination and tube elongation (Cole, *et al.*, 2005; Hála *et al.*, 2008; Bloch *et al.*, 2016; Li *et al.*, 2017). The rules by which various secretory cargos are packaged and trafficked, and how these cargos become incorporated into a functional wall upon secretion, remains poorly understood, however. The PT is an excellent system for studying these processes given its rapid growth, heavy dependence on secretion and the importance of maintaining proper cell wall organization in these cells.

We have previously shown that successful PT elongation and fertilization requires protein glycosylation, specifically of the hydroxyproline *O*-arabinosylation (Hyp-Ara) type (MacAlister *et al.*, 2016). *O*-linked protein glycosylation, like Hyp-Ara, begins in the ER with the conversion of peptidyl proline to Hyp by prolyl-4 hydroxylases (Adams and Frank, 1980). In plants, Hyp can be modified by *O*-linked glycosylation in the form of Hyp-Ara or Hyp *O*-(arabino)galactosylation (Tan *et al.*, 2010; Showalter and Basu, 2016). The type of modification a given Hyp receives depends on the protein context: contiguous and non-contiguous Hyps are arabinosylated, whereas clustered but discontinuous Hyps, like those occurring in the arabinogalactan proteins, are galactosylated (Kieliszewski and Shpak, 2001; Ohyama *et al.*, 2009). For Hyp-Ara, arabinose sugars are sequentially added until a linear chain of up to four or five sugars is formed (Lamport and Miller, 1971). The first, (β-1,4-linked) arabinofuranose is added by the Golgi-localized HYDROXYPROLINE *O*-ARABINOSYLTRANSFERASE 1–3 (HPAT1–3) enzymes, which are classified as glycosyltransferase family GT95 members (Ogawa-Ohnishi *et al.*, 2013). The single arabinose (Hyp-Ara_1) may then be extended by the GT77 family members REDUCED RESIDUAL ARABINOSE 1–3 (RRA1–3) and XYLOGLUCANASE113 (XEG113), which add a second (β-1,2-linked) and a third (β-1,2-linked) arabinofuranose, respectively (Egelund *et al.*, 2007; Gille *et al.*, 2009; Velasquez *et al.*, 2011). The fourth (α-1,3-linked) arabinofuranose is added by the GT47-classified EXTENSIN ARABINOSE DEFICIENT TRANSFERASE (ExAD) (Møller *et al.*, 2017). Enzyme activity for the addition of the rare fifth arabinose has not yet been assigned. In the absence of HPAT activity, Hyp-oligoarabinosides are not produced (MacAlister *et al.*, 2016). In Arabidopsis, mutants of the three-member *HPAT* gene family have reported pleiotropic effects, including reduced hypocotyl length, reduced cell wall thickness, accelerated senescence in *hpat1 hpat2* double mutants and disrupted root hair elongation (Ogawa-Ohnishi *et al.*, 2013; Velasquez *et al.*, 2015). *HPAT1* and *HPAT3* are redundantly required for full male fertility: *hpat1 hpat2 hpat3* triple mutants and *hpat1 hapt3* double mutants display low male fertility and PT growth defects, leading to reduced male transmission and low seed set (MacAlister *et al.*, 2016).

The largest known group of HPAT-target proteins are members of the EXTENSIN (EXT) family of repetitive cell wall structural glycoproteins (Lamport, 1967; Lamport and Miller, 1971; Brownleader and Dey, 1993; Showalter *et al.*, 2010). Following heavy Hyp-Ara modification, EXTs are secreted into the apoplast, where they assemble into an insoluble covalent network by peroxidase-mediated cross-linking of tyrosine residues (Held *et al.*, 2004; Everdeen *et al.*, 1988). The glycosylation of the EXTs contributes to their rod-like, extended poly-Pro-II left-handed helical conformation, and increases tyrosine cross-linking *in vitro* (van Holst and Varner, 1984; Stafstrom and Staehelin, 1986a; Stafstrom and Staehelin, 1986b; Chen *et al.*, 2015). This EXT network is hypothesized to serve as scaffolding for further cell wall assembly, specifically through acid–base and/or covalent interactions with pectins (Qi *et al.*, 1995; Cannon *et al.*, 2008). Proteins with EXT-like regions fused to other domains are also predicted to carry Hyp-Ara modifications. These 'EXT-chimeras' have many proposed functions, with the EXT-like region generally proposed to act in cell wall binding or sensing. EXT-chimeras include the leucine-rich repeat extensin (LRX) proteins, the proline-rich extensin-like receptor kinase (PERK) proteins and the class-I formin homology (FH) proteins (Showalter *et al.*, 2010; Borassi *et al.*, 2016).

With the aim of understanding the requirement for Hyp-Ara in PT growth, we carried out a genetic suppressor screen to identify additional factors in the HPAT pollen fertility pathway. Here, we report on the cloning and characterization of two such suppressor mutants, both of which encode members of the exocyst complex, pointing to an important link between the regulation of secretion, protein glycosylation and cell wall structure in the PT.

RESULTS

To identify mutations suppressing the pollen fertility defect of *hpat1 hpat3* double mutants (*hpat1/3*, for brevity), we mutagenized approximately 2000 *hpat1/3* seeds by treatment with 0.2% ethyl methanesulfonate. Self-fertilized progeny were screened for increased silique length and seed set (see Experimental procedures). The suppressor mutants identified, named *fertility restored in hpat1/3* (*frh*), were confirmed to be homozygous for the original *hpat1* and *hpat3* insertion mutations, and to display consistently increased fertility between generations and following backcrosses with the parental strain.

frh1 improves the fertility of *hpat1 hpat3* pollen

In contrast to the *hpat1/3* genetic background, suppressed *frh1 hpat1/3* plants showed increased silique length and higher seed set, but appeared otherwise morphologically normal (Figure 1). To confirm that *frh1* suppression was the result of improved pollen fertility we analyzed seed set following reciprocal crosses between the suppressed line and *hpat1/3*. The *hpat1/3* fertility defect is limited to the pollen; seed set can be fully rescued by pollination with wild-type (WT) pollen (MacAlister *et al.*, 2016). Similarly, seed set was high when *frh1 hpat1/3* was used as the pollen parent, but not when it was used as the seed parent with *hpat1/3* pollen, demonstrating that the suppression in *frh1* resulted from increased pollen fertility (Figure 1b). This enhanced pollen fertility coupled with the Arabidopsis habit of producing excess pollen, relative to ovule number, impacted the genetic behavior of *frh1 hpat1/3* and its pattern of inheritance. Seed set was significantly increased in both homozygous and heterozygous (i.e. backcross F_1) *frh1 hpat1/3* plants (Figure 1b). In *frh1/+ hpat1/3*, the increased fitness of pollen carrying the *frh1* mutation also drove high *frh1* male transmission and reduced the number of non-suppressed progeny recovered. In a backcross F_2 population, only 9% of plants displayed low, *hpat1/3*-like fertility, a significant deviation from the 25% expected in the absence of any transmission bias ($n = 123$; χ^2-test, $P = 1.55 \times 10^{-5}$).

Given that *frh1* improved *hpat1/3* pollen fertility *in vivo*, we next analyzed the phenotype of *frh1 hpat1/3* PTs directly. When grown on *in vitro* pollen germination media, *hpat1/3* PTs displayed a number of defects, including reduced PT length, the initiation of secondary tips (i.e. 'branched' PTs), high frequencies of PT rupture and modestly increased PT width. We found *frh1* partially suppressed all of these defects (Figure 1d,e and Figure S1). Interestingly, we also found that *frh1 hpat1/3* pollen germinated at a lower frequency than either WT or *hpat1/3* pollen. The apparent reduction in germination in *hpat1/3* is at least partially a result of poor PT growth. *hpat1/3* PTs often rupture and can do so before a tube becomes sufficiently apparent to consider a pollen grain germinated. This was not true for *frh1 hpat1/3* pollen grains, however, which had a reduced frequency of PT rupture but a further reduced germination frequency. In a comparison of sustained PT growth rates for each genotype, we found an overall reduction in *hpat1/3* PTs that was suppressed by *frh1* (Figure S1i). Although the *frh1 hpat1/3* growth rate was even higher than the WT rate, this did not translate into an increase in the overall length of PTs after 5 h of growth (Figure 1d). We also noted that *hpat1/3* PTs would often arrest growth for extended periods of time before ultimately rupturing. The average duration of this pre-rupture pausing was 24.5 min and ranged from less than 5 min to longer than 100 min ($n = 11$).

frh1 does not restore Hyp-Ara, but partially rescues cell wall organization

The most direct mechanism for suppressing the *hpat1/3* phenotype would be restoration of the Hyp-Ara protein modification itself. In order to assess the Hyp-Ara status of *frh1*, we sought an antibody capable of specifically recognizing this modification. The extensin (EXT) family of cell wall structural proteins is known to be heavily Hyp-Ara modified and several monoclonal antibodies have been previously raised against purified EXTs. We tested three of these for Hyp-Ara specificity (JIM11, JIM19 and JIM20; Smallwood *et al.*, 1994; Smallwood *et al.*, 1995). We found that JIM20 recognized protein samples from WT seedlings, but not from *hpat* triple-mutant seedlings, which we have previously shown to lack detectable Hyp-Ara (Figure S2a,b; MacAlister *et al.*, 2016). Furthermore, JIM20 did not recognize protein from mutants of the arabinosyltransferases, adding the second and third 1 → 2-linked β-arabinofuranoses (the *rra2 rra3* double mutants and the *xeg113-3* mutant; Egelund *et al.*, 2007; Gille *et al.*, 2009). JIM20 did, however, recognize protein from *exad1-1* plants; therefore, the fourth, 1 → 3-linked α-arabinofuranose added by ExAD is not required for JIM20 recognition (Møller *et al.*, 2017). We immuno-labeled pollen grains and PTs with JIM20 to determine the localization of Hyp-Ara in these cells. We found robust staining of the WT pollen grain and tube cell wall (Figure 2a, Figure S2c). In *hpat1/3* pollen, we detected no JIM20 signal, as in WT secondary antibody alone controls (Figure S2d,e). As in *hpat1/3*, no Hyp-Ara was detected in *frh1 hpat1/3* tubes (Figure S2f). Therefore, *frh1* did not suppress the *hpat1/3* phenotype by directly restoring Hyp-Ara, but through another mechanism.

The *hpat1/3* pollen phenotypes are consistent with defective cell wall integrity. In order to gain insight in the molecular basis for these defects, and the suppression of these defects in *frh1*, we compared the organization of key PT cell wall polymers. Given the importance of pectin for PT growth and the proposed function of EXTs in pectin organization, we hypothesized that compromised EXT

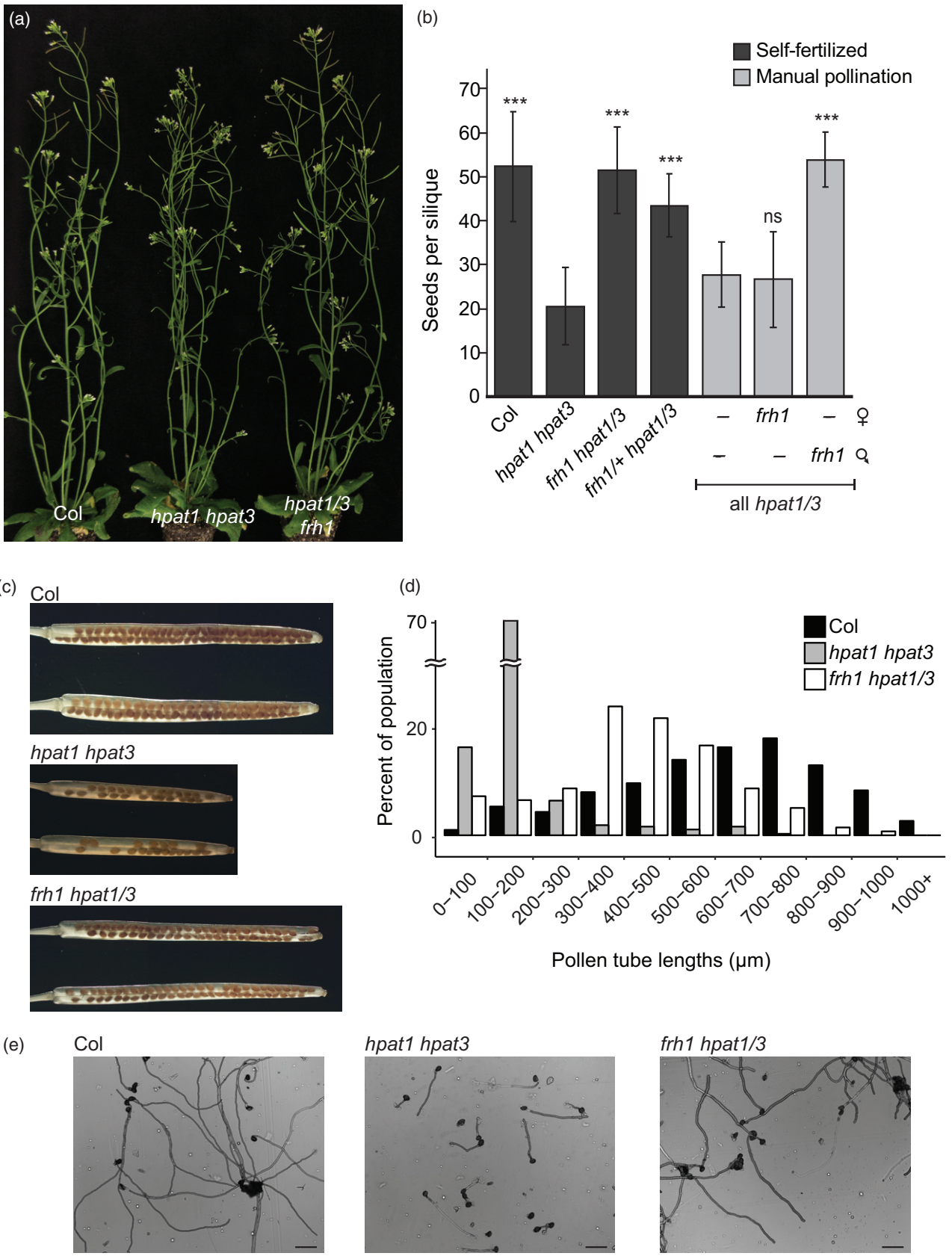

Figure 1. Suppressor mutant *frh1* increases the pollen fertility of *hpat1 hpat3* plants.
(a) Both double mutant *hpat1/3* plants and the suppressed triple mutant *frh1 hpat1/3* plants appeared morphologically normal, aside from differences in seed set. (b) Average number of seeds per silique (±SD, $n \geq 10$ per genotype) for the indicated genotypes. The low-seed-set phenotype of *hpat1/3* double mutants is suppressed by *frh1*. High seed set is also observed for heterozygous *frh1* plants. Reciprocal crosses between *hpat1/3* and *frh1 hpat1/3* plants demonstrated that *frh1* suppression occurs in the pollen. ***Statistically significant difference (Student's *t*-test, $P < 0.0005$) compared with the *hpat1/3* value for either the self-fertilized siliques or the manually pollinated samples. NS is not significantly different. (c) Cleared siliques of wild-type (WT) Columbia, *hpat1 hpat3* and *frh1 hpat1/3* plants. WT and *frh1 hpat1/3* images are composite images to allow full silique imaging. (d) Histogram of distribution of pollen tube (PT) lengths after 5 h of *in vitro* growth for the indicated genotypes. Data for all genotypes are statistically significantly different from both other genotypes (Student's *t*-test, $P < 0.005$). (e) *In vitro* grown PTs of the indicated genotypes. Scale bars: 100 μm.

Hyp-Ara may alter pectin distribution in the cell wall. We used the monoclonal antibodies LM19 and LM20 (Verhertbruggen *et al.*, 2009) to assess the distribution and abundance of demethyl-esterified homogalacturonan (dme-HG) and methyl-esterified HG (me-HG), respectively, in WT, *hpat1/3* and *frh1 hpat1/3* PTs. A key functional difference between these two forms of pectin is their ability to form calcium salt bridges. dme-HG is able to form a cross-linked structure, whereas the methyl-ester groups present on the me-HG prevent this (Micheli, 2001). In WT PTs, the me-HG recognized by LM20 was enriched at the PT tip, whereas the calcium cross-linkable dme-HG recognized by LM19 was excluded from the tip and enriched in the shaft, consistent with previous reports (Figure 2c,d; Bosch and Hepler, 2005; Dardelle *et al.*, 2010; Rounds *et al.*, 2011; Chebli *et al.*, 2012). This pattern was disrupted in *hpat1/3* PTs. The LM20 epitope (me-HG) signal enrichment at the tip region was weaker in *hpat1/3*. Moreover, the overall level of LM19 epitope (cross-linkable dme-HG) was increased in the shaft region and enriched rather than excluded from the tip (Figure 2c,d). *frh1 hpat1/3* PTs had intermediate levels of dme-HG (LM19) signal, however, and reduced me-HG (LM20) at the tip relative to the shaft, although the pattern was not restored to that of the WT.

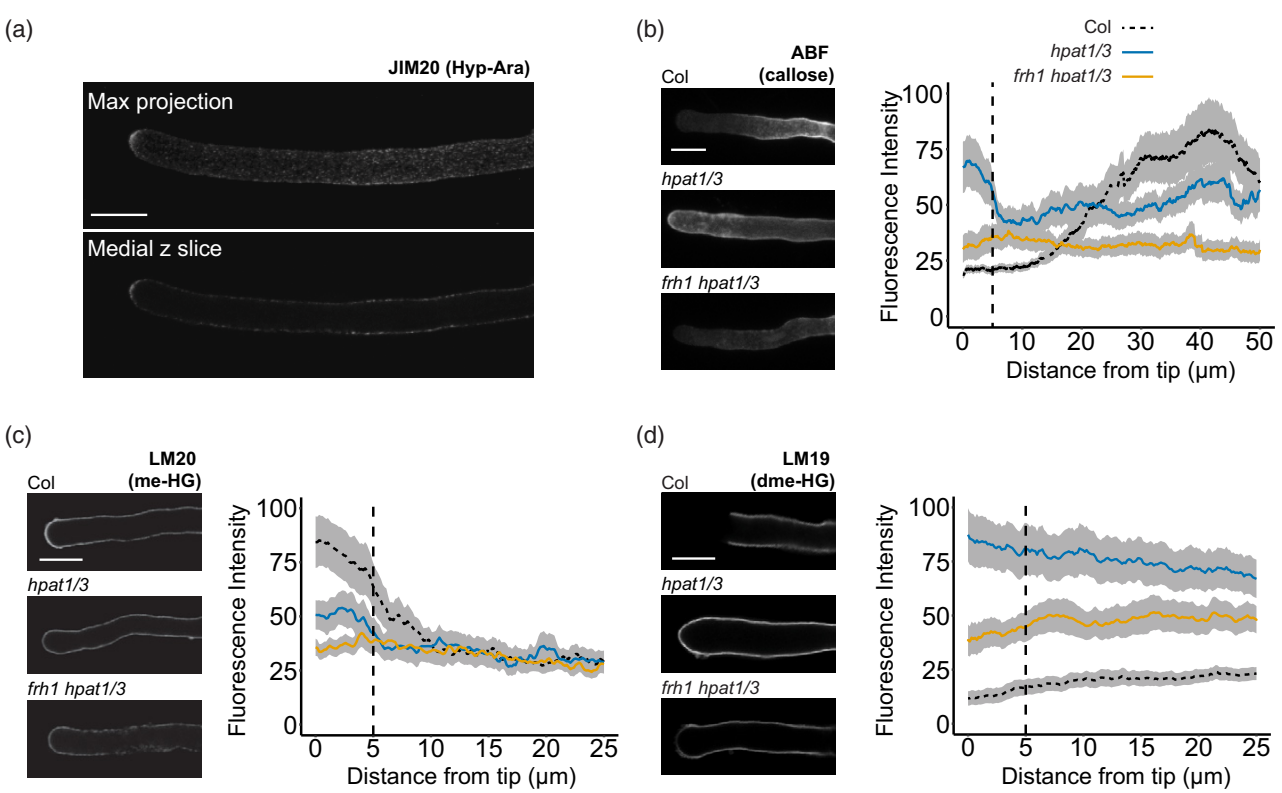

Figure 2. *frh1* partially suppresses the disrupted polarity of cell wall polymers in *hpat1/3* pollen tubes (PTs).
(a) Wild-type (WT) Columbia-0 PT stained with JIM20 primary antibody and anti-rat FITC-conjugated secondary antibody. (b) Left: Maximum projections of PTs stained with aniline blue fluorochrome (ABF). Right: quantification of signal intensity from the tip (distance on *x*-axis = 0) to 50 μm down the shaft of the PT (for more details concerning image analysis, see Experimental procedures). Colored lines represent the mean fluorescent intensities for each genotype, and shading represents the standard error. $n \geq 30$ for each genotype. The vertical dashed line represents the approximate region of the PT where the apical dome transitions to the shaft. (c) Left: medial *Z*-slices of PTs stained with LM20 primary antibody and anti-rat FITC-conjugated secondary antibody. Right: quantification of fluorescence intensity as in (b), except measurements were taken to 25 μm from the tip. (d) Left: medial *Z*-slice of PTs stained with LM19 primary antibody and anti-rat FITC-conjugated secondary antibody. Right: quantification of signal intensity as in (c). All images were acquired by confocal microscopy at 100× magnification. Scale bars: 10 μm.

Increased cell wall rigidity at the PT tip in *hpat1/3* through the accumulation of dme-HG in this region is consistent with the poor expansion ability of this genotype. The reduced accumulation of this polymer in *frh1* is also consistent with its improved growth and the suppressed phenotype. Interestingly, in *frh1 hpat1/3* PTs, the tip enrichment of me-HG (LM20 signal) was almost completely missing and the expression was generally flat across the length of the PT (Figure 2c).

The PT shaft is also reinforced with callose (Schlupmann *et al.*, 1994; Van der Woude *et al.*, 1971). We stained PTs with aniline blue fluorochrome (ABF) to compare callose distribution between genotypes. As expected, in WT PTs we found high levels of ABF binding along the shaft and low signal at the tip. Again, consistent with the poor expansion ability of *hpat1/3* pollen, we found high levels of ABF signal at the PT tip. This enrichment was abrogated in *frh1 hpat1/3* tubes, although not restored to WT levels, again, consistent with the improved growth of suppressed PTs (Figure 2b).

frh1 suppression is caused by a mutation in *exo70a2*

To identify the mutation conferring increased seed set and improved PT growth in *frh1* plants, we used a high-throughput sequencing strategy (Beuder and MacAlister, 2020). *frh1* was backcrossed to the parental strain for four generations and allowed to self-fertilize, forming the BC4 F_2 generation. To identify homozygous *frh1* individuals for sequencing, the BC4 F_2 plants were used as females in test crosses with *hpat1/3* pollen. Homozygous *frh1* plants produce only suppressed F_1 progeny, whereas heterozygous females produce a 1:1 ratio of suppressed and non-suppressed progeny. A minimum of 11 test cross progeny per parent were scored for 25 BC4 F_2 individuals. Twelve were found to be homozygous (100% suppressed progeny, $n = 149$ total), whereas the remaining 13 were heterozygous (49.4% suppressed progeny, $n = 170$ in total). We extracted DNA from three groups of plants: the self-fertilized progeny of the confirmed homozygous *frh1* plants (the *frh1/frh1* pool), the non-suppressed progeny segregating from the heterozygous plant test crosses (the *FRH1/FRH1* pool) and the *hpat1/3* genetic background.

Following paired-end 150-bp DNA sequencing, quality control and read mapping, we identified sequence variants from all three DNA samples relative to the Columbia reference genome (Table S1). From the variants identified in the *frh1/frh1* data, we removed all variants shared with the background strain (*hpat1/3*) or the *FRH1/FRH1* pool, leaving 18 287 unique *frh1* variants. We filtered this set for single-nucleotide polymorphisms, as expected for an ethyl methanesulfonate (EMS)-induced mutation, supported by a minimum of four reads, leaving 16 001 variants. After filtering for a minimum variant sequence read frequency of 80%, we were left with 48 variants, eight of which were predicted missense mutations. Thirty of these variants were clustered within a 5.7-Mbp region on chromosome 5, presumably containing the causative mutation and those linked to it (Table S2). Near the middle of this region, we identified a missense mutation converting glycine 319 to a glutamic acid in EXO70A2, a predicted subunit of the vesicle-tethering exocyst complex. The altered amino acid position (glycine 319) is conserved in eight of the 23 Arabidopsis EXO70s, including the A, E, F and G subfamilies, and is directly C-terminal to a phenylalanine that is conserved in all Arabidopsis EXO70s (Figure S3).

We tested for co-segregation between the *exo70a2*^{G319E} variant (hereafter *exo70a2-2*) and the suppressive phenotype in an *frh1* BC5 F_2 population using a polymerase chain reaction (PCR)-based genotyping assay. As expected for the causative mutation, we found a significant bias against recovery of homozygous wild-type plants and perfect concordance between the *exo70a2-2* genotype and suppressive phenotype, including intermediate seed-set values for heterozygous plants (Figure S4). To confirm that the *exo70a2* mutation is the cause of the suppression in *frh1*, we expressed the wild-type genomic *EXO70A2* sequence from a transgene in the *frh1 hpat1/3* background. Transgenic *frh1* 'rescue' would be a return to the low fertility of the *hpat1/3* parental strain. We cloned a 3971-bp region of the EXO70A2 locus including the native promoter, full coding region and approximately 450 bp of

Figure 3. *EXO70A2* is required for efficient pollen germination and pollen tube (PT) growth.
(a) Diagram of the *EXO70A2* coding sequence, with the position of the *exo70a2-2* (G319E) missense mutation and insertion mutants *exo70a2-D* (Hála *et al.*, 2008) and *exo70a2-3* marked. (b) Semi-quantitative RT-PCR of flower cDNA samples from the indicated genotypes showing an absence of transcript in the *exo70a2-3* plants using the primer pairs indicated in (a). (c) Average number of seeds per silique (±SD) for plants of the indicated genotype. Note the modest reduction in seed set for *exo70a2-3* in the wild-type (WT) background along with the partial suppression of the *hpat1 hpat3* phenotype by this mutation. ***Statistically significant differences with the corresponding background (Columbia or *hpat1 hpat3*, Student's *t*-test, $P < 0.0005$, $n \geq 12$). (d) Cleared siliques of the *exo70a2* mutant alleles in the Columbia background, see Figure 1(d) for Col comparison image. (e and f) *In vitro* pollen germination samples of Columbia (e) and *exo70a2-3* (f) 3 h after transfer to growth media. Inset in (f) shows non-germinated *exo70a2-3* pollen grains. (g) Quantification of pollen germination frequencies for WT, *exo70a2-2* and *exo70a2-3*. Mean of three replicates of ≥740 pollen grains, ±SD. **Significant difference between WT (Student's *t*-test, $P < 0.005$). (h–j) Alexander viability staining of anthers of WT (h), *exo70a2-2* (i) and *exo70a2-3* (j). Insets show free pollen grains. Note no difference in viability staining between genotypes. (k and l) Pollen grains stained with Ruthenium red to mark pectin accumulation at the germination plaque. (m) Histogram of PT lengths after 5 h of *in vitro* growth for the indicated genotypes. Data for all genotypes are statistically significantly different from both other genotypes (Student's *t*-test, $P < 0.005$, $n \geq 200$ per genotype). (n) sustained growth rate of PTs of the indicated genotype. Mean, $n \geq 21$ tubes, ±SD. (o and p) Differential interference contrast (DIC) micrograph of PTs.

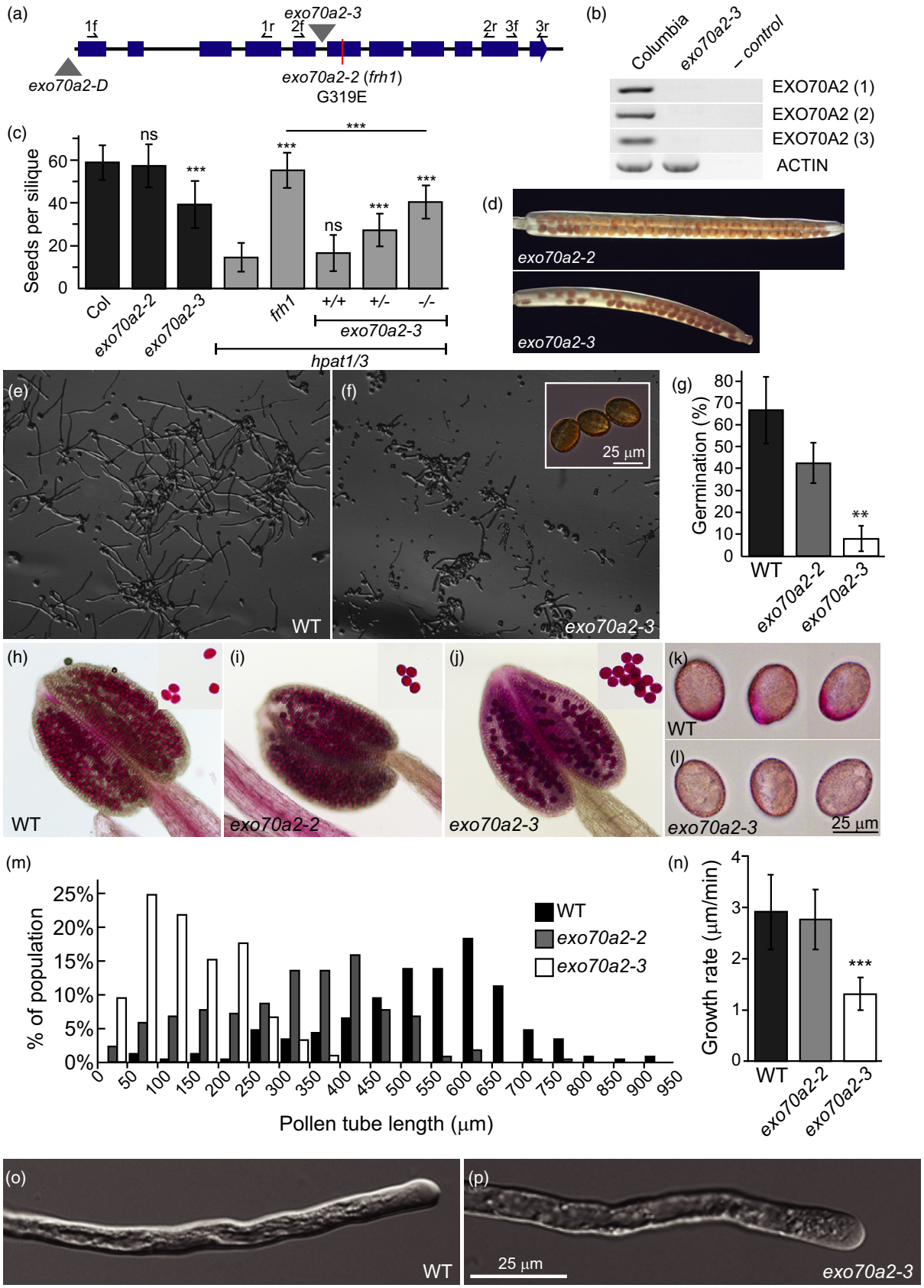

3′ sequence and recombined this fragment into a plant expression vector containing a seed-expressed fluorescent transformation marker (Shimada *et al.*, 2010). We compared the transgene transmission efficiency in three independent single-loci insertion hemizygous lines and found a significant and robust male-specific transmission defect for the *EXO70A2* transgene for all lines (Figure S5). The same plasmid backbone carrying a strong pollen-specific promoter (Lat52) driving expression of the florescent protein, mNeonGreen, had no effect on male or female transmission (Figure S5b; Bate and Twell, 1998; Shaner *et al.*, 2013). Furthermore, in *exo70a2-2 hpat1/3* lines homozygous for the transgene, seed set was reduced to the level of the *hpat1/3* background, whereas non-transgenic sibling plants had a *frh1*-like high level of seed set (Figure S5c), thus confirming that the *exo70a2-2* mutation confers the increased fertility observed in *frh1 hpat1/3* plants.

EXO70A2 is required for efficient pollen germination and pollen tube growth

Given the effect of *exo70a2-2* on *hpat1/3* pollen fertility, we next determined the phenotypic consequence of this mutation in an otherwise WT background. From a Col outcross population, we isolated *exo70a2-2* homozygous mutants that were wild type for *HPAT1* and *HPAT3*. We observed no statistically significant change in seed set between Columbia and *exo70a2-2* (Figure 3c); however, using a more sensitive competitive fertilization assay, we found significantly reduced male transmission of the *exo70a2-2* allele versus the WT allele (16.7% transmission efficiency, $n = 84$; χ^2-test, $P = 5.89 \times 10^{-11}$). Therefore, in an otherwise WT background, *exo70a2-2* reduced pollen fitness.

As we had observed the partial rescue of cell wall organization in suppressed PTs (Figure 2), we compared the PT cell wall organization between the WT and *exo70a2-2*. We again used LM19 and LM20 to compare the distribution of dme-HG and me-HG, respectively, along with ABF staining to compare callose accumulation. In all three cases, the overall pattern of signal was similar between WT and *exo70a2-2* tubes (Figure S6). The only difference we observed was an overall reduction of signal intensity for LM19 (dme-HG) in *exo70a2-2*, although the pattern of low signal at the tip and increasing signal in the shaft was the same for both genotypes. We next used the JIM20 antibody to compare distribution of Hyp-Ara. Similar to our observations for LM19 staining, the overall intensity of JIM20 signal was reduced in *exo70a2-2* PTs, although the pattern was generally flat across the PT length in both genotypes. Therefore, although *exo70a2-2* partially restores PT cell wall organization in the *hpat1/3* background, it did not alter cell wall polarity in the wild-type background.

Our transgenic rescue data (Figure S5) suggest that the G319E allele is likely to be a loss- or reduction-of-function allele, and the only previously published allele (*exo70a2-D*) is a promoter-region insertion with increased transcript expression with no reported pollen fertility phenotypes (Synek *et al.*, 2017). To gain further insight into the function of this gene, we identified an additional allele with an insertion in the fifth intron of *EXO70A2* among the available insertion mutant collections. Based on reverse transcriptase (RT)-PCR analysis of flower cDNA, we found that this insertion mutant (*exo70a2-3*) was a transcriptional null allele (Figure 3b). Seed set was modestly reduced in homozygous *exo70a2-3* plants compared withthe WT background (Figure 3c,d), and the male transmission efficiency of *exo70a2-3* was also reduced to about half of the value in *exo70a2-2* (8.3% transmission efficiency; $n = 130$; χ^2-test, $P = 5.03 \times 10^{-22}$). We next tested *exo70a2-3* for suppression of the *hpat1/3* low-fertility phenotype. Self-fertilized progeny of *exo70a2-3/+ hpat1/3* plants displayed a significant bias towards inheritance of the *exo70a2-3* mutant allele, consistent with a suppressive effect conferring improved transmission of the triple-mutant pollen (13% WT, 49% heterozygous, 37% homozygous mutant; $n = 67$ total; χ^2-test, $P = 7.06 \times 10^{-9}$). Seed set in *hpat1/3 exo70a2-3* triple mutants was also significantly increased compared with the *hpat1/3* background, although the *exo70a2-3* allele did not increase seed set to the same degree as the *exo70a2-2* allele (Figure 3c).

As *exo70a2* mutants exhibit reduced male fitness in the wild-type background, we analyzed their pollen phenotypes directly. When grown *in vitro* we observed a moderate and strong reduction in pollen germination frequency for *exo70a2-2* and *exo70a2-3*, respectively (Figure 3e–g). The non-germinated pollen grains appeared morphologically normal and all pollen appeared similarly viable based on Alexander staining (Figure 3h–j; Peterson *et al.*, 2010). We hypothesize the observed germination defect resulted from a failure to target secretory vesicles to the germination site, similar to the pollen germination defect described for other exocyst mutants, including *sec3a,* sec6, *sec8, sec15a* and *sec5* (Cole *et al.*, 2005; Hála *et al.*, 2008; Bloch *et al.*, 2016; Li *et al.*, 2017). We examined germination plaque formation using Ruthenium red, which stains pectin accumulation (Li *et al.*, 2017). Although WT pollen accumulated pectin at the germination site as expected, most *exo70a2-3* pollen did not, consistent with the low germination frequency in this line (Figure 3k,l). We further noted that the mutant pollen that successfully germinated produced shorter PTs than the wild type after 5 h of growth (Figure 3m), although they were otherwise morphologically normal (Figure 3o,p). To determine whether this was the result of slower rates of PT growth or an indirect effect of delayed germination, we measured the sustained PT growth rate. Following successful germination,

exo70a2-3 PTs elongated at about half the rate observed in the WT, although the rate of *exo70a2-2* PT growth was not significantly different from that of the WT (Figure 3n). Therefore, *exo70a2* mutants have both impaired pollen germination and tube elongation, phenotypes consistent with a secretion defect, with the *exo70a2-3* null allele being more severely impaired than the missense allele *exo70a2-2*.

EXO70A2 *localizes to the tip of growing pollen tubes*

The microarray, mRNA sequencing and proteomic data available indicate that *EXO70A2* is most strongly, if not exclusively, expressed in pollen and PTs (Hruz *et al.*, 2008; Grobei *et al.*, 2009; Klepikova *et al.*, 2016; Synek *et al.*, 2017). To validate this expression data and determine the subcellular localization of EXO70A2, we generated a C-terminal mNeonGreen fusion protein including the native promoter region and full genomic sequence (EXO70A2-mNG). In stably transformed wild-type plants, we observed reporter expression in *in vitro* grown PTs, with no detectable expression in other tissues, in agreement with the reported expression data. To determine whether the fusion protein was functional, we transformed homozygous *exo70a2-3* plants with this construct. In contrast to the low germination frequency of *exo70a2-3* pollen, pollen from three independent T_1 plants had a significantly higher proportion of germinated pollen grains after 2 h and the vast majority of T_1 PTs were positive for mNeonGreen fluorescence, demonstrating that pollen carrying the reporter construct was able to germinate and form elongating PTs, whereas the non-transgenic mutant pollen largely failed to do so (Figure S7). A similar experiment using the EXO70A2^{G319E} point mutant fused to mNeonGreen resulted in a much weaker rescue of pollen germination frequency, suggesting that this mutant is a hypomorph with reduced activity relative to the wild-type sequence (Figure S7b). In addition to the weaker rescue by the mutant protein, the resulting PTs had noticeably weaker fluorescence than the corresponding wild-type EXO70A2-mNG expression lines, suggesting that the mutant protein may be less stable *in vivo*, potentially accounting for its lower activity.

In budding yeast, EXO70p localizes to the target membrane, along with SEC3p, through phospholipid interactions, and recruits the remaining vesicle-associated complex members to the site of tethering (Liu *et al.*, 2007; He *et al.*, 2007a). Given the importance of proper vesicle targeting during tip growth, we examined the localization of the EXO70A2:mNG fusion protein in PTs and observed signal at the tip plasma membrane (Figure 4). This localization pattern was similar to the immunolocalization pattern reported by Hála *et al.* (2008) in *Nicotiana tabacum* (tobacco) PTs using an antibody raised against the highly similar EXO70A1. Furthermore, a C-terminal YFP fusion to the tobacco EXO70A2 homolog (NtEXO70A2) was reported to localize to the PT tip, but only occasionally to show PM localization (Sekereš *et al.*, 2017).

exo70a2 mutants reduce Hyp-Ara modified protein secretion at the pollen tube tip

The localization of EXO70A2 to the PT tip (Figure 4), combined with the reduced pollen germination and slower PT growth of *exo70a2-3* mutants (Figure 3), suggested that EXO70A2 is a positive regulator of PT tip growth and is likely to act as a canonical exocyst complex member. Therefore, we hypothesized that the suppression of *hpat1/3* by *exo70a2* mutants was caused by reduced rates of secretion of one or more key exocyst cargo(s). Hyp-Ara modified proteins themselves are a strong candidate for exocyst-mediated secretion. To develop a secretion reporter to allow us to follow Hyp-Ara modified proteins, we used a portion of a directly validated HPAT substrate, EXT3 (Ogawa-Ohnishi *et al.*, 2013), specifically an arabinosylation motif (SPPPP) and an adjacent sequence (KSPPPPVKHLY) inserted into an exposed loop of GFP (Figure 5a). Insertion into the GFP sequence has been shown to stabilize glycoprotein fusions, which are otherwise often subject to terminal tag cleavage and degradation (Yang *et al.*, 2012). We used the EXT3 signal peptide sequence to

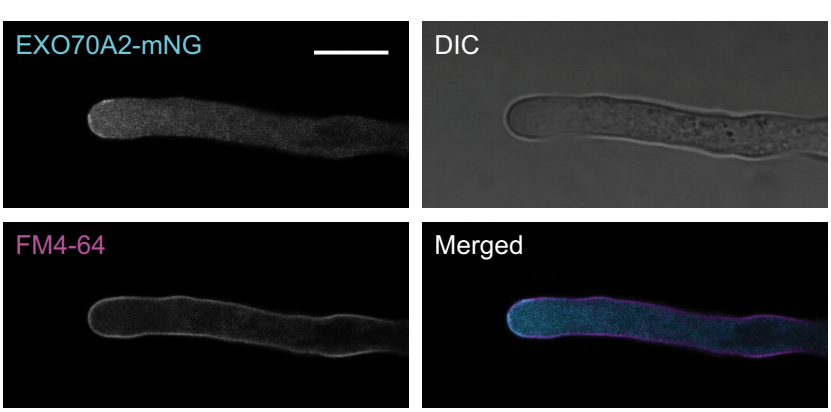

Figure 4. EXO70A2 localizes to the tip of growing pollen tubes (PTs).
Representative PT expressing *EXO70A2:mNG* under its native promoter and co-stained with FM4-64 to visualize the plasma membrane. Single channels and merged image shown; overlapping signal is false-colored white. Imaged with confocal microscopy at 100× magnification. Scale bar: 10 μm.

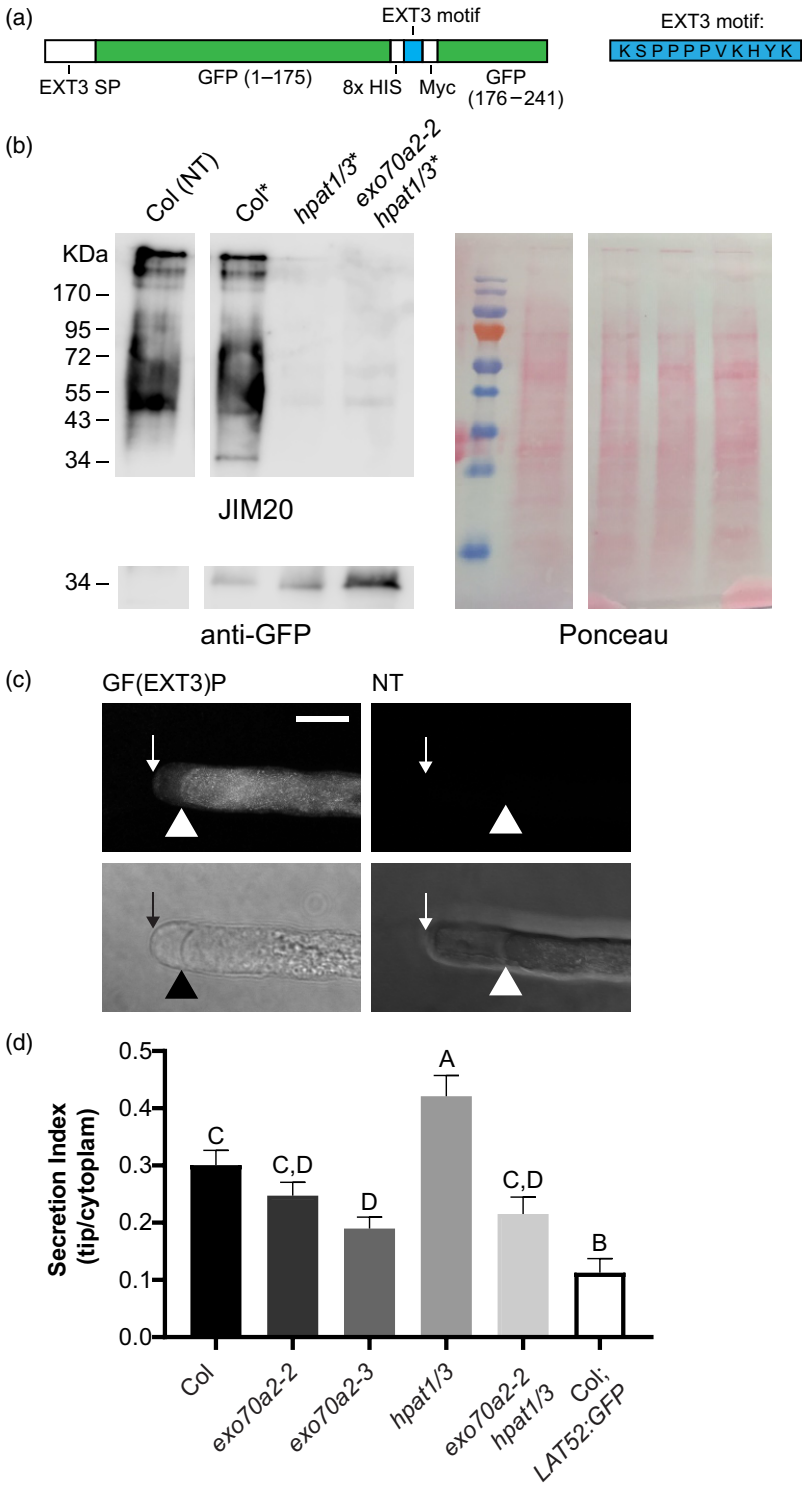

Figure 5. Secretion of GF(EXT3)P is decreased in *hpat1/3 exo70a2-2* pollen tubes (PTs).
(a) Schematic of the GF(EXT3)P construct, which includes the EXT3 signal peptide (SP), amino acids 1–175 of GFP, an 8× HIS tag, a portion of EXT3, a Myc tag, and amino acids 176–241 of GFP. (b) Western blots (left) and corresponding Ponceau-stained membrane (right) of PT protein samples. *Samples from plants carrying the *LAT52:GF(EXT3)P* transgene; NT, non-transgenic. An anti-GFP polyclonal antibody detects the fusion protein in the transgenic lines at the expected mass (~34 kDa). The reporter is also detected by the Hyp-Ara monocolonal antibody JIM20 only in the transgenic Col sample. (c) Images of plasmolyzed PTs expressing *LAT52:GF(EXT3)P* (left) and non-transgenic control (right). Scale barL 10 μm. Arrows indicate the location of the PT cell wall tip, and arrowheads mark the plasma membrane. (d) Quantification of secreted GFP signal reported as a secretion index (SI: mean ± SE, $n \geq 30$ PTs per genotype; for details, see Experimental procedures). Samples labeled with the same letter are not significantly different (Benjamini–Hochberg flase-discovery rate, FDR ≤ 0.05).

drive the protein into the secretory pathway and expressed the resulting fusion, GF(EXT3)P, under the Lat52 promoter for pollen expression (Bate and Twell, 1998). We stably transformed this construct into *hpat1/3* plants. To limit potential confounding effects resulting from expression-level variation between independent transgenic lines, we crossed a single, robustly expressing *hpat1/3* GF(EXT3)P line to Col, *exo70a2-2*, *exo70a2-3* and *hpat1/3 exo70a2-2*, and isolated the desired genotypes from the resulting F_2 populations. As a control, we also transformed a GFP construct with no signal peptide (Lat52::GFP) into Col.

We were able to detect GF(EXT3)P from PT protein samples with an anti-GFP polyclonal antibody at the expected molecular mass of the fusion, approximately 34 kDa (Figure 5b). To determine whether the fusion protein was arabinosylated, we probed with the JIM20 Hyp-Ara antibody. No native arabinosylated proteins of the GF(EXT3)P mass were observed in untransformed Col PTs, but we detected JIM20 signal at the observed reporter mass in the GF (EXT3)P transgenic Col line (Figure 5b). No JIM20 signal was detected from *hpat1/3* or *exo70a2-2 hpat1/3* transgenic samples, consistent with the absence of Hyp-Ara in these genotypes.

In *in vitro* grown GF(EXT3)P-expressing PTs, we observed robust intracellular fluorescence, likely linked to the presence of the reporter in the secretory pathway (ER, Golgi and secretory vesicles). To determine whether the protein was secreted, we plasmolyzed PTs by transfer to high-sucrose media. In PTs, plasmolysis occurs preferentially at the tip region, separating the plasma membrane from the cell wall (Hill *et al.*, 2012). We observed fluorescence signal remaining at the vacated PT tip, suggesting that the protein was secreted into the cell wall space (Figure 5c). To quantitatively compare secretion between genotypes, we calculated a 'secretion index' (SI) as a ratio of fluorescence intensity of the cytoplasm-free tip region to the intracellular signal after subtraction of the non-tube background. The Col GF(EXT3)P SI was significantly higher (approx. threefold greater) than that of the control GFP construct, demonstrating that the GF (EXT3)P construct was actively secreted (Figure 5d). This secretion was also partially dependent on *EXO70A2*; the SI was significantly lower in *exo70a2-3* compared with WT PTs, although it was still greater than the SI of the control (Figure 5e). Interestingly, the SI was increased by approximately 40% in *hpat1/3* mutants compared with Col, suggesting more rapid secretion of HPAT-target proteins in the absence of the HPATs, despite the lower growth rate of the *hpat1/3* tubes (Figure S1i). Finally, we found that SI was significantly reduced in the suppressed *hpat1/3 exo70a2-2* PTs, compared with *hpat1/3*, but did not significantly differ from the *exo70a2-2* value. Thus, in addition to the cell wall defects of *hpat1/3* PTs noted above, increased secretion of unmodified HPAT-target proteins may be further confounding the cell wall structure of the mutant PTs.

sec15a mutants also suppress the *hpat1/3* fertility phenotype

The data above suggest an important function for *EXO70A2* in the secretion of glycoproteins in PTs. The *exo70a2* mutant phenotypes were also consistent with the defects observed for mutants in other exocyst complex members (Cole, *et al.*, 2005; Hála *et al.*, 2008; Li *et al.*, 2017 and Bloch *et al.*, 2016). If the underlying mechanism of *hpat1/3* suppression by *exo70a2* is a reduction of exocyst-mediated secretion, mutants in other members of the core exocyst should also suppress the *hpat1/3* fertility defects. Fortuitously, in the course of sequencing additional *frh* suppressor lines, we identified a line carrying a mutation in exocyst complex member *SEC15A,* converting serine 213 to phenylalanine (Figure 6a; Table S3). *SEC15A* is one of two Arabidopsis *SEC15* genes and is required for male transmission, pollen germination and PT growth (Hála *et al.*, 2008). In the BC5 F_2 generation of this suppressor family, we found strong bias against the recovery of plants homozygous for the wild-type *SEC15A* allele, as expected for an *hpat1/3*-suppressing mutation (Figure 6b,c; χ^2-test, $P = 1.57 \times 10^{-5}$). Following pollination of *hpat1/3* pistils by pollen from *sec15a-3/+ hpat1/3* plants, 90% of the progeny inherited the *sec15a-3* allele (61 heterozygous versus seven WT progeny; χ^2-test, $P = 5.8 \times 10^{-11}$), confirming increased male transmission of the *sec15a*^{S213F} mutation (hereafter *sec15a-3*) in the *hpat1/3* background. We also found perfect co-segregation between *sec15a-3* and the suppressive phenotype, including intermediate seed-set values for heterozygous individuals (Figure 6d). Like *exo70a2-2*, the *sec15a-3* mutant also increased PT lengths *in vitro* in the *hpat1/3* background (Figure 6e). After outcrossing our suppressor allele to the wild-type Columbia background to remove the *hpat1* and *hpat3* mutations, *sec15a-3* mutants did not display significantly different seed set compared with the WT, similar to our observations for *exo70a2-2* (Figures 6d and 3c). The transmission efficiency of the mutant allele was reduced in the WT background (TE = 60.6%; $n = 249$; χ^2-test, $P = 1.1 \times 10^{-4}$), however, indicating a modest fertility cost to pollen carrying the mutant allele.

Given that loss-of-function *exo70a2* mutants were able to suppress the *hpat1/3* phenotype, we reasoned that the suppression by *sec15a-3* was also caused by a loss of function of this core exocyst complex member. Therefore, we next crossed *hpat1/3* to a previously published transcription null T-DNA insertion allele of *sec15a* (*sec15a-2*, SALK_067498; Hála *et al.*, 2008). In plants homozygous for the *hpat1* and *hpat3* mutations, the presence of a *sec15a-2* allele increased seed set with homozygous *sec15a-2* plants being more strongly impacted (Figure 6d), thus confirming

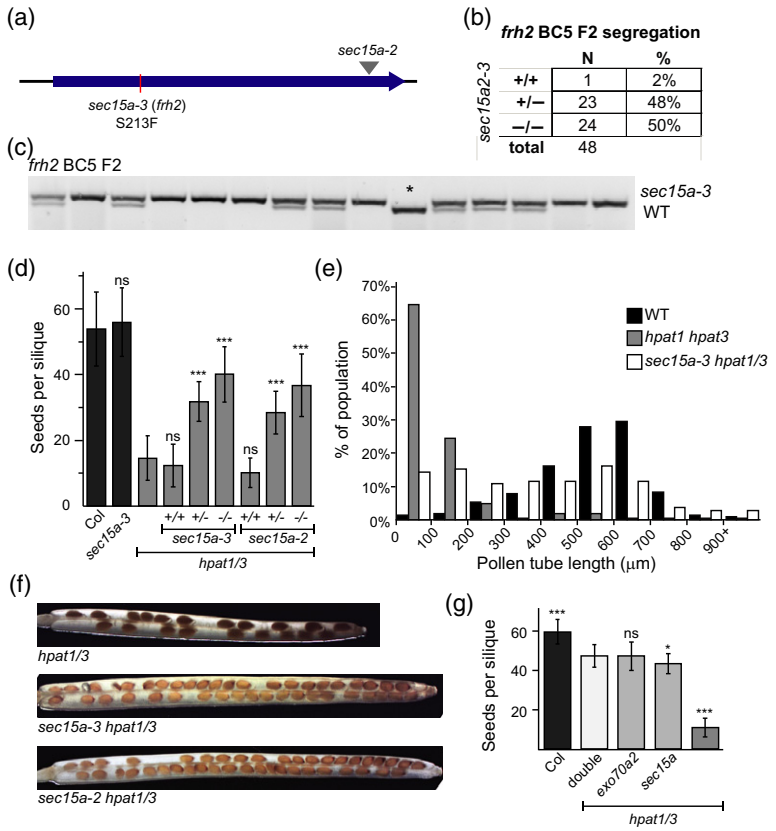

Figure 6. Mutations in exocyst complex member *sec15a* also suppress the *hpat1/3* fertility phenotype.
(a) Gene model diagram showing the relative position of insertion in the *sec15a-2* allele and the suppressor allele identified in *frh2* (*sec15a-3*). (b) Segregation of the *sec15a-3* mutation in the *frh2 hpat1/3* BC5 F_2 population. As expected for an *hpat1/3*-suppressing mutation, the number of homozygous wild-type *SEC15A* plants identified (+/+) was significantly below the expected value based on Mendelian segregation (chi-square test, $P = 1.57 \times 10^{-5}$). (c) Sample *sec15a-3* genotyping data for 15 *frh2 hpat1/3* BC5 F_2 individuals visualized on an agarose gel. The wild-type (WT) allele is cleaved by digestion with *Mnl*I. The single homozygous WT individual marked by '*' did not have the suppressive phenotype. (d) Average number of seeds per silique (±SD) for plants of the indicated genotypes. *sec15a-2* is not transmitted through the male and is not recoverable as a homozygous mutant (Hála *et al.*, 2008). Both *sec15a* alleles suppress the *hpat1/3* phenotype, with homozygous mutants showing stronger suppression than heterozygotes. 'ns' marks samples that were not statistically different from their corresponding background genotype. ***Statistically different samples (Student's *t*-test, $P < 0.0005$, $n \geq 11$). (e) Histogram of PT lengths after 5 h of *in vitro* growth for the indicated genotypes. Data for all genotypes are statistically significantly different from both other genotypes (Student's *t*-test, $P < 0.005$, $n \geq 100$ per genotype). (f) Cleared siliques of the indicated genotypes. (g) Average number of seeds per silique (±SDs) for the indicated genotypes. All *hpat1/3*-based genotypes were siblings segregating from the same F_2 population. Statistically different samples (Student's *t*-test): ***$P < 0.0005$; *$P < 0.05$ ($n \geq 15$).

that the loss of function of *sec15a* can suppress the *hpat1/3* phenotype. The recovery of homozygous *sec15a-2* plants in the *hpat1/3* background was somewhat surprising, as this allele is essential for male transmission in the WT background (Hála *et al.*, 2008).

If *exo70a2* and *sec15a* both suppress the *hpat1/3* fertility defect through disruption of the same protein complex, plants carrying both mutations should exhibit no further suppression relative to the single suppressor mutants. We crossed the two suppressor families to establish the genetic relationship between them. In the double suppressor genotype (i.e. *hpat1/3 exo70a2-2 sec15a-3* quadruple mutants) we observed the same level of seed set as sibling *hpat1/3 exo70a2-2* plants and a minor, but statistically significant (Student's *t*-test, $P = 0.03$) increase compared with the *hpat1/3 sec15a-3* siblings (Figure 6g), consistent with the hypothesis that both suppress through the disruption of the core exocyst complex.

DISCUSSION

Pollen tubes (PTs) grow by the targeted secretion of new cell wall material to their tip. We have previously shown that the plant-specific protein modification hydroxyproline *O*-arabinosylation (Hyp-Ara) is required for proper PT growth and full male fertility (MacAlister *et al.*, 2016). Here, we report major changes in the organization of the PT cell wall in *hpat1/3* mutants, specifically a loss of PT cell wall polarity and the conversion of the normally extensible cell wall structure at the PT tip into a more shaft-like state (Figure 2). Although immunolocalization studies of cell wall epitopes must be interpreted with caution because of potential epitope masking by interaction between

polymers, our results demonstrate a change in cell wall organization in the *hpat1/3* PTs. Once the tip wall is disrupted, as in the *hpat1/3* tubes, one would expect cell expansion to be compromised, leading to growth arrest and/or PT rupture. The 'branching' observed for *hpat1/3* PTs may be the result of growth being re-directed to a more viable subapical cell wall region (Figure S1). The EXT family of cell wall structural glycoproteins are heavily Hyp-Ara modified; therefore, the most direct explanation for the disrupted cell wall organization of the *hpat1/3* PTs is that the lack of Hyp-Ara prevents proper EXT function in the cell wall, broadly disrupting cell wall organization. The unmodified EXTs may also be toxic to cell wall structure, with their presence as un-arabinosylated proteins causing greater disruption to the wall than their absence would. Loss-of-function mutants of the exocyst components *exo70a2* and *sec15a* suppress the *hpat1/3* pollen fertility phenotype, suggesting that reducing the rate of secretion of one or more key exocyst cargos allows *hpat1/3* PTs to compensate for their defects. This is apparent as a partial restoration of PT cell wall organization, specifically a reduction of the anomalous accumulation of dme-HG and callose at the PT tip (Figure 2), and as an increased PT growth rate (Figure S1i).

To determine whether HPAT-modified proteins themselves are trafficked through the exocyst, we generated a Hyp-Ara modified secreted reporter: GF(EXT3)P. The SI of GF(EXT3)P was significantly reduced in PTs of the null *exo70a2-3* allele compared with WT PTs (Figure 5), indicating that reporter secretion was, at least partially, *EXO70A2* dependent. The *exo70a2-3* GF(EXT3)P SI was still above the SI of the GFP control, however. Thus, there may be exocyst-independent secretion of GF(EXT3)P or functional redundancy within the 23 members of the *EXO70* gene family. Several other *EXO70* genes are expressed in PTs and two (*EXO70C1* and *EXO70C2*) have demonstrated PT functions, although their mutant phenotypes are qualitatively distinct from those of other exocyst complex mutants, suggesting that they may be regulators of exocyst function rather than canonical exocyst components (Hruz *et al.*, 2008; Chong *et al.*, 2009; Grobei *et al.*, 2009; Li *et al.*, 2010; Klepikova *et al.*, 2016; Synek *et al.*, 2017). A recent preprint characterizing a CRISPR/Cas9 induced *exo70a2* mutant allele agrees with our findings with respect to the importance of *EXO70A2* for pollen germination and PT elongation, further supporting its central role in PT exocytosis (Marković *et al.*, 2019). Furthermore, the reduced secretion of Hyp-Ara modified proteins in *exo70a2* mutants would also be consistent with the reduced levels of JIM20 staining we observed in *exo70a2-2* PTs (Figure S6). The reduced SI of the GF(EXT3)P reporter in the *exo70a2* mutant indicates that the protein is being retained cytoplasmically. This retention may be occurring in secretory vesicles, at earlier points in the secretory pathway (e.g. the Golgi apparatus), or in another compartment. Determining the site of retention will require co-localization with subcellular markers. We also found that *hpat1/3* PTs had the highest GF(EXT3)P SI of any genotype (Figure 5). Enhanced secretion of a glycoprotein in the absence of the relevant glycosyltransferases has been previously noted in other systems, although the underlying mechanism remains unknown. For example, in budding yeast, mutation of mannosyltransferases required for N-linked hypermannosylation of cell wall glycoproteins resulted in increased secretion of modified heterologous proteins (Tang *et al.*, 2016). The knock-down of Golgi stacking proteins also led to reduced glycosylation and accelerated secretion (Xiang *et al.*, 2012). The underlying cause of increased glycoprotein secretion in *hpat1/3* is unclear. Partial arabinosylation could serve as a Golgi retention signal, preventing premature target protein secretion, and as the *hpat1/3* PTs cannot initiate arabinosylation, such a retention signal would be absent. Alternatively, the presence of the HPAT enzymes themselves may be required for target protein retention. The *hpat1* and *hpat3* alleles are transcriptional nulls (MacAlister *et al.*, 2016), and thus any protein–protein interactions that they participate in would be disrupted in *hpat1/3* mutants. Alternatively, other compensation pathways may be activated in the *hapt1/3* PTs, leading to an indirect increase in secretion. Regardless of the cause of the elevation in *hpat1/3* PTs, the secretion index was significantly reduced in *exo70a2-2 hpat1/3* PTs.

Although the GF(EXT3)P secretion reporter showed that the secretion rate was altered for a synthetic HPAT-modified protein, determining which native protein(s) are important for PT growth is more difficult. The list of candidate proteins for HPAT-modification is long, and includes the 20 classical Arabidopsis EXTs and multiple EXT-chimera families, including the LRX, PERK and class-I FH proteins (Showalter *et al.*, 2010; Choudhary *et al.*, 2015; Johnson *et al.*, 2017). Several members of each of these gene families are expressed in pollen. For example, six members of the *PERK* family of 15 genes are highly or exclusively expressed in pollen samples in Arabidopsis (Borassi *et al.*, 2016). The class-I FH genes, *FH3* and *FH5*, are also expressed in pollen and are known to be important regulators of PT growth through their regulation of the actin cytoskeleton (Cheung and Wu, 2004; Ye *et al.*, 2009; Cheung *et al.*, 2010). The *LRX* genes include four members (*LRX8-11*) that are expressed specifically in pollen and have been shown to redundantly contribute to pollen fertility. Higher-order *lrx* mutants displayed reduced pollen germination, abnormal PT morphology and frequent tube rupture (Fabrice *et al.*, 2018; Sede *et al.*, 2018; Wang *et al.*, 2018). LRX proteins have also been shown to bind to the RALF4/19 peptides and participate in an autocrine signaling loop, maintaining PT

integrity until reaching the ovule (Mecchia *et al*., 2017). Furthermore, Fabrice *et al*. (2018) also demonstrated reduced levels of JIM20 signal in *lrx8/9* and *lrx8/9/11* mutant PTs. This could be interpreted as a direct reduction in Hyp-Ara in these mutants arising from reduced LRX protein levels, although an indirect effect involving feedback with other modified proteins cannot be ruled out.

In addition to the EXTs and EXT-chimeras, a second unrelated group of HPAT-modified proteins is currently known: the small secreted signaling peptides of the CLAVATA 3/EMBRYO-SURROUNDING REGION-RELATED (CLE) family. Mutants of HPAT family members from *Solanum lycopersicum* (tomato), *Medicago truncatula* and *Lotus japonicus* function in the regulation of shoot meristem size and the determination of nodule number through their effect on CLE peptide arabinosylation (Schnabel *et al*., 2011; Xu *et al*., 2015; Kassaw *et al*., 2017; Imin *et al*., 2018; Yoro *et al*., 2019). Although the participation of an HPAT-modified CLE peptide in PT growth is an intriguing possibility, no candidates for such a pollen-expressed CLE are forthcoming (Kanaoka and Higashiyama, 2015).

Moreover, although we demonstrated reduced secretion of a Hyp-Ara modified reporter protein in the suppressed PTs (Figure 5d), this does not preclude the trafficking of other cargos through the exocyst. Slowing the delivery of cell wall polysaccharides or non-arabinosylated cell wall modifying enzymes may also contribute to *hpat1/3* suppression by exocyst mutants. In the PT, pectins are initially secreted in the methylesterified form and then de-methylesterified in the wall by pectin methyl esterases (PMEs), which are in turn regulated by PME inhibitors (PMEIs; Bosch and Hepler, 2005). Altering the rate of delivery of pectin, PME and/or PMEI proteins could alter the timing of de-methylesterification in the PT wall. There is evidence of exocyst involvement in pectin secretion in the specialized seed coat mucilage cells (Kulich *et al*., 2010). The exocyst is also involved in the secretion of cellulose synthase complexes (Zhu *et al*., 2018) and may be trafficking other, similar complexes in the PT (e.g. callose synthases).

Evidence is mounting that secretion is likely to be more complex than a simple bulk flow of Golgi material to the plasma membrane. Data from budding yeast has shown distinct post-Golgi secretory vesicles carrying different sets of cargos marked by the presence of Bgl2p or invertase, with mutations in *exo70* predominantly blocking the secretion of Bgl2p-containing vesicles (Harsay and Bretscher, 1995; He *et al*., 2007b). In plant cells there is also evidence of distinct trafficking pathways for reporter proteins versus cell wall polysaccharides (Leucci *et al*., 2007). The trafficking landscape of PTs is likely to be complex and subject to tight regulation.

EXPERIMENTAL PROCEDURES

Plant growth conditions and materials

Arabidopsis thaliana plants of the Columbia-0 ecotype were grown under 16-h light/8-h dark cycles in a temperature-controlled growth room maintained at 23°C. The recovery of *hpat1-2* (Salk_120066) *hpat3-1* (Salk_085603) double mutants has been described previously (MacAlister *et al*., 2016). *frh* mutants were induced by treatment of *hpat1/3* seeds with 0.2% EMS for 12 h. Seeds from the mutagenized plants were collected in pools of 5–10 M_1 plants and approximately 96 M_2 individuals per pool were screened for increased silique length and higher seed content. *frh* candidates were genotyped for the *hpat1* and *hpa3* mutant alleles to confirm homozygosity and were backcrossed to the *hpat1/3* background for four generations. The *exo70a2-3* (WiscDsLoxHs216_02A; Woody *et al*., 2007) and *sec15a-2* (SALK_067498; Alonso *et al*., 2003) insertion alleles were obtained from the Arabidopsis Biological Resource Center (ABRC, https://abrc.osu.edu). Mutants were genotyped using the primers listed in Table S4. RT-PCR for *exo70a2-3* knock-out validation used the *EXO70A2* primers given by Synek *et al*. (2017) and primers from Table S4. The *rra2* (SAIL_244_A03), *rra3* (Gabi 223B05), *xeg113-3* (SALK_058092) and *exad1-1* (SAIL_843_G12) insertion alleles were genotyped using the primers listed in Table S4. To clear siliques for seed counts, fully expanded but unripe siliques were transferred to 70% ethanol for at least 2 days, after which time the ethanol was replaced with 50% glycerol for several more days.

Whole-genome sequencing

After four generations of backcrossing of the *frh* plants to *hpat1/3*, suppressed F_2 plants were crossed as females to *hpat1/3* plants to identify homozygous and heterozygous individuals based on suppression segregation in the cross progeny. Self-fertilized seeds from confirmed homozygous BC4 F_2 plants were germinated on MS media plates for DNA extraction, as were seeds of the *hpat1 hpat3* background strain. Tissue for the FRH/FRH pool was collected from non-suppressed plants produced by the heterozygous test cross progeny. DNA was extracted from the tissue pools using the Qiagen Plant DNA Mini kit (Qiagen, https://www.qiagen.com), according to the manufacturer's instructions, followed by concentration by ethanol precipitation. Libraries were generated using Illumina TruSeq DNA kits (Illumina, https://www.illumina.com) and barcoded for multiplexing by the University of Michigan DNA Sequencing Core. Samples were sequenced on the Illumina HiSeq-4000 platform with paired-end 150-bp cycles. Sequence reads were checked for quality using FASTQC then aligned with the TAIR10 genome using BOWTIE 2, and sequence variants

were called using FREEBAYES. Additional analysis steps were performed with SAMTOOLS. We identified all the mutations in each suppressor family and removed mutations that were also present in the *hpat1/3* and/or the FRH/FRH samples. We then filtered the mutations based on an allelic frequency ≥ 0.8, mutation type = single-nucleotide polymorphism (SNP) and read number ≥ 4. We annotated the sequence variants for context and predicted effect using a custom PERL script.

JIM20 dot blot and Western blot analysis

Total non-covalently-bound protein was extracted from Col, *hpat1/2/3*, *rra2/3*, *xeg113* and *exad* seedlings grown on MS plates using a procedure modified from Fry (1988). Tissue was ground in liquid nitrogen and resuspended in freshly prepared solution A (100 ml of acetic acid, 250 ml of 80% w/w phenol), stirred rapidly in a fume hood at 70°C for 30 min, and cooled prior to filtering through GF/C glass fiber paper in a 4.25-cm porcelain Buchner funnel (VWR 470153-508; VWR, https://www.vwr.com). The residue was rinsed twice with 5 ml of solution B (35 ml of solution A, 5 ml of H_2O) and then 2.5 ml of 10% ammonium formate. After that, 255 ml of acetone was added to the filtrate and incubated on ice for an hour. The protein precipitate was spun in PYREX™ round-bottom glass centrifuge tubes (05-558-5B; FisherScientific, https://www.fishersci.com) for 5 min at 2500 ***g***, the supernatant discarded and the pellet resuspended in 10 ml of 10% acetone. After a second spin for 5 min at 2500 ***g***, the protein was resuspended as far as possible in a minimal volume of H_2O (1–5 ml) and its concentration determined using a bicinchoninic acid (BCA) protein assay kit (23225; Pierce, now ThermoFisher Scientific, https://www.thermofisher.com). For dot blots, 5 μg of total protein extract was spotted onto 0.2 μm nitrocellulose and allowed to dry prior to immunoprocessing. For western blots, 15 μg of total protein extract was separated by 10% mini-PROTEAN® TGX™ (456-1033; Bio-Rad, https://www.bio-rad.com) gel electrophoresis and transferred onto a 0.2-μm polyvinylidene difluoride (PVDF) membrane (170-4156; Bio-Rad, now ThermoFisher Scientific) using the Trans-Blot® Turbo™ transfer system. Dot blots and western blots were then blocked for 1 h (5% milk, in 1× Tris-Buffered Saline with Tween [150 mM NaCl, 20 mM Tris base, 0.1% Tween 20; TBST]), probed with 1:10 JIM20 monoclonal rat IgM primary antibody (Carbosource, https://www.ccrc.uga.edu) in blocking buffer in a sealed polypropylene envelope overnight at 4°C, washed three times with 1× TBST for 10 min, probed with goat anti-rat IgG H + L secondary antibody (PI31629; FisherScientific), washed twice with 1× TBST for 10 min, once with 1× TBS for 10 min, treated with chemiluminescent substrate (WBKLS0500; Immobilon, https://www.emdmillipore.com) and analyzed on CL-XPosure film (34090; FisherScientific).

Pollen assays

All pollen germination and growth assays were carried out using *in vitro* pollen growth media (PGM), modified from Rodriguez-Enriquez *et al.* (2013), composed of 10% sucrose, 0.01% boric acid, 1 mM $CaCl_2$, 1 mM $Ca(NO_3)_2$, 1 mM KCl, 0.03% casein enzymatic hydrolysate, 0.01% myo-inositol, 0.1 mM spermidine, 10 mM γ-aminobutyric acid, 500 μM methyl jasmonate, pH adjusted to 8.0, and solidified with 1% low melting temperature agarose. The agarose was dissolved by slow heating on a 100°C stir plate and the media was poured into 35-mm Petri plates. When solidified, the media was covered with a piece of cellophane. To germinate and grow PTs *in vitro*, pollen from recently opened flowers was dusted directly onto the cellophane and the PGM plates were placed in a humid chamber consisting of a plastic box with damp paper towels. For PT length measurements, pollen was allowed to grow for 5 h before tubes were imaged with a dissecting microscope equipped with a camera. PTs were measured using IMAGEJ (https://imagej.nih.gov). For PT width measurements, PTs were imaged on a compound microscope using a 20× objective after 3 h of growth *in vitro*. Three measurements were made across the width of each tube ≥10 μm from the pollen grain and tip using IMAGEJ. The measurements were averaged to generate a single width measurement per tube. To determine PT rupture frequency, PTs were imaged after 3 h of growth and the number of ruptured tubes was divided by the total number of PTs analyzed.

To measure PT growth rates, pollinated PGM plates were immobilized in 100 mm × 15 mm Petri dishes with double-sided tape, and pieces of damp paper towel were placed in the larger petri dish to maintain high humidity. These plates were then placed directly on the stage of a dissecting microscope (equipped with a camera) and not moved for 3 h of imaging. To determine sustained growth rates, images of the same field of PTs were taken at 20-min intervals. PT lengths were measured at each time point, the change in length was calculated and the growth rate was determined by dividing this by the number of minutes between images. The growth rates from every interval of every PT for each genotype was averaged to generate an overall 'global' growth rate value. At least 30 PTs were analyzed for each genotype. To determine the length of pre-rupture growth stalling in *hpat1/3* PTs, the above procedure was followed with the imaging interval reduced to 5 min and the time of rupture noted.

Protein extraction from pollen tubes and Western blot analysis

Protein extraction from PTs was performed as described by Chang and Huang (2017), with slight modifications. Flowers were collected in 1.5-ml microcentrifuge tubes and

suspended in 1 ml of agarose-free PGM. The tubes were vortexed for 1 min and incubated at room temperature (20–23°C) in the dark for 3–5 h with agitation. Flower debris was removed with forceps and PTs were collected by centrifugation at 16 000 *g* for 2 min. The supernatant was removed and the pollen pellet tube was placed on ice. Using a polypropylene pestle, the pellet was ground for 1 min and then incubated in K-HEPES protein extraction buffer buffer (20 mM HEPES, pH 7.0, 110 mM K-acetate, 2 mM $MgCl_2$, 0.1% Tween 20, 0.2% Triton X-100, 1 mM phenylmethylsulfonyl fluoride, PMSF) for 1 h on ice. The tubes were then centrifuged at 22 000 *g* for 20 min. The soluble fraction in the supernatant was removed and the insoluble fraction/pellet was resuspended in 2× Laemmli sample buffer with β-mercaptoethanol, diluted 1:1 with K-HEPES buffer, and then heated to 95°C for 10 min. For Western blots, the insoluble protein extract was separated by sodium dodecyl sulfate polyacrylamide gel electrophoresis (SDS-PAGE) (15% polyacrylamide) and transferred onto a nitrocellulose membrane using the Trans-Blot® Turbo™ transfer system. Membranes were then blocked for 1.5 h with 5% milk in 10× TBST and probed with either 1:10 JIM20 monoclonal rat IgM primary antibody (Carbosource) or 1:1000 anti-GFP polyclonal rabbit IgG (Life Technologies, now ThermoFisher Scientific, https://www.thermofisher.com) in blocking buffer in a sealed polypropylene envelope overnight at 4°C with agitation. The next day, membranes were washed three times with 1× TBST for 10 min, probed with either goat anti-rat horseradish peroxidase (HRP)-conjugated secondary antibody (for JIM20) or anti-rabbit HRP-conjugated secondary antibody (for anti-GFP), sealed in a polypropylene envelope and incubated at room temperature for 1.5 h with agitation. Membranes were then washed twice with 1× TBST for 10 min, once with 1× TBS for 10 min, treated with chemiluminescent substrate (SuperSignal West Femto Maximum Sensitivity Substrate) for 5 min and imaged with a LI-COR Odyssey Fc Dual-Mode Imaging System (LI-COR, https://www.licor.com).

Cloning

For the transgenic rescue construct, the *EXO70A2* gene was amplified from Columbia-0 in a single fragment including the native promotor (376 bp), coding region and the 3′ sequence up to the first predicted polyadenylation site using the primers in Table S4 with Phusion® High-Fidelity DNA Polymerase (M0530S; NEB, https://www.neb.com). For C-terminal fusion to mNeonGreen, the *EXO70A2* sequence was amplified from the promoter to the last coding codon from either Columbia-0 or the *exo70a2-2* mutant. The resulting fragments were cloned into Gateway® entry clones via BP Clonase II™ (11789-020; Invitrogen, now ThermoFisher Scientific, https://www.thermofisher.com). The transgenic rescue construct was recombined via LR Clonase II™ (11791-020; Invitrogen, now ThermoFisher Scientific) into the pFAST-G01 binary vector (Shimada *et al.*, 2010) and the localization reporters were recombined into a modified pFAST-R07 vector, in which the GFP sequence was replaced with mNeonGreen. As a result of restriction-site limitations, a portion of the pFAST-R07 vector was amplified, using the Phusion® High-Fidelity DNA Polymerase (M0530S; NEB) alongside the mNeonGreen fusion protein, and the two fragments joined by overlap extension PCR. The GFP sequence was removed from pFAST-R07 by *Nru*I and *Mlu*I restriction digestion and the mNeonGreen-containing fragment inserted using T4 DNA Ligase (M1801; Promega, https://www.promega.com) to make pFAST-mNG.

The GF(EXT3)P construct was generated through the following steps. *pPS48-35SPro-GF-Muc1-P-35S-term* is an intermediate vector previously assembled for embedded *GFP* cloning (Yang *et al.*, 2012), where the signal sequence (*At*SS) was derived from the N-terminal signal peptide sequence of *A. thaliana* basic endochitinase B (P19171; Uniprot, https://www.uniprot.org). First, the *GF-Muc1* fragment was obtained by *Pst*I/*Bam*HI double digestion and used as template for PCR with primers FReplace and RReplace. The resulting GF-Muc1 fragment was cloned into the multiple cloning site of pPS48. The two EXT3 encoding oligos pYi1 and pYi2 were inserted into the *Nco*I/*Bam*HI site of the pPS48 vector. The entire fragment CaMV35S-*At*SS-GF(EXT3)P-NosTerm was excised using *Xba*I and ligated into pGreen0179, yielding the plant expression plasmid pGreen0179-35SPro-*At*SS-GF(EXT3)P-NosTerm. The *At*SS sequence in this construct was substituted with the signal sequence of EXT3 (At1g21310) by In-Fusion cloning (638933; TaKaRa, https://www.takarabio.com), using the primer sets p162 and p164 on *35SPro-At*SS-*GF(EXT3)P-NosTerm* to obtain the fragment containing the *35S* promoter from pGreen and EXT3 signal peptide overlap, and the primer sets p163 and p165 on *35SPro-AtSS-GF(EXT3)P-NosTerm* to obtain signal peptide overlap, and embed GFP and the *35S* terminator. The vector fragment was obtained from V26 (pUC57, including synthetic gene fragments and AttL sites, obtained from Genescript, https://www.genscript.com) digested with *Spe*I and *Xba*I for directed insertion of *35SPro-EXT3ss* and *EXT3ss-GF(EXT3)P-NosTerm* into the vector fragment using the In-Fusion Cloning kit. The LAT52 promoter for pollen expression was amplified from tomato genomic DNA using the primers listed in Table S4. The EXT3ssGF(Ext3)P fragment was amplified from the *EXT3ss-GF(EXT3)P-NosTerm* plasmid, incorporating attB2 and attB5 sites in the forward and reverse primers, respectively: GF(EXT3)P F and GF(EXT3)P R. The LAT52pro and EXT3ssGF(EXT3)P fragments were cloned into their respective Gateway® entry vectors via BP Clonase II™ (11789-020; Invitrogen, now ThermoFisher Scientific). The LAT52pro and EXT3ssGF(EXT3)P entry clones were

combined with the pFAST-G01 vector (Shimada *et al.*, 2010) by two-fragment recombination using LR Clonase II™ (11791-020; Invitrogen, now ThermoFisher Scientific). The control LAT52:GFP construct was generated by one-fragment LR Clonase II™ (11791-020; Invitrogen, now ThermoFisher Scientific) recombination between a LAT52-pro entry vector and pFAST-G07, which contains the GFP coding sequence (Shimada *et al.*, 2010).

Microscopy

For immunolocalization, PTs were fixed, imaged and analyzed as described by Chebli *et al.* (2012), with several modifications. PTs were grown in agarose-free PGM for at least 2 h, then the media with PTs was transferred to a 12-mm × 75-mm polystyrene culture test tube. PTs were collected by centrifugation at 20 *g* for 2 min with low acceleration and deacceleration, and then the growth media was removed. For fixation, PTs were resuspended in 3.5% formaldehyde in piperazine-N,N′-bis(2-ethanesulfonic acid) (PIPES) buffer (50 mM PIPES, 1 mM ethylene glycol-bis(β-aminoethyl ether)-N,N,N′,N′-tetraacetic acid, 5 mM $MgSO_4$, 0.5 mM $CaCl_2$, pH 7) and vacuum infiltrated for 20 min. After fixation, PTs were washed three times with PIPES buffer and then three times with phosphate-buffered saline (PBS) + 3% bovine serum albumin (BSA). After the final wash, PTs were resuspended in primary antibody and incubated at 4°C overnight with gentle agitation. Primary antibodies were diluted in PBS + BSA to the following concentrations: JIM20, 1:5; LM19, 1:10; and LM20, 1:5 (antibodies obtained from PlantProbes, http://www.plantprobes.net). The next day the tubes were spun down and primary antibody was removed, and then the PTs were washed three times in PBS + BSA. Anti-rat fluorescein isothiocyanate (FITC)-conjugated secondary antibody (diluted 1:100 in PBS + BSA) was added, and the tubes were incubated at room temperature in the dark for 2 h. After incubation, PTs were washed three times with PBS followed by three washes with DI water. PTs were then resuspended in mounting media (0.1% gelatin and 10% ethanol), transferred to slides with a pipette and the slides were stored overnight in the dark at room temperature to allow PTs to settle onto the mounting media. The next day, VectaShield was added to the slides, covered with a #1.5 coverslip, sealed with nail polish and stored at 4°C.

Imaging was performed with a Leica SP5 laser-scanning confocal microscope. To image the FITC signal, we used a 488-nm excitation laser, an RSP500 dichroic beam splitter (Leica, https://www.leica-microsystems.com) and detectors that were set to capture light with a wavelength range of 495–600 nm. For each different experiment the imaging settings, including laser intensity, gain, line averaging and frame accumulation, were adjusted so that the signal from the overall brightest tube was just below saturation; all images for a single experiment were taken with identical settings. *Z* stacks were taken throughout the entire volume of each PT. The *Z*-slice step sizes were automatically optimized and maximum-intensity projections were generated using LAS-AF, with $n \geq 30$ PTs used for each genotype. Images were analyzed using IMAGEJ. To measure fluorescence signal intensities, a line was drawn using the segmented line tool along the periphery of the PT, starting from the center of the PT tip towards the pollen grain, or as far as possible. Two measurements were performed for each PT along each periphery/side. The PLOT PROFILE tool in IMAGEJ was used to measure the pixel gray value along distance, with distance = 0 representing the tip apex. For a single PT, the values of each side were averaged to generate a single measurement, and the measurements of all PTs were averaged within each genotype.

For aniline blue staining, PTs were grown *in vitro* on PGM plates with cellophane for 2 h. A drop of 0.1 mg ml^{-1} aniline blue fluorochrome (ABFC; Biosupplies Australia Pty. Ltd., http://www.biosupplies.com.au) diluted 1:70 in 0.1 M KH_2PO_4, pH 10, was added to a microscope slide, and PTs were transferred to the slide by dabbing the cellophane on the ABFC solution. Nail polish was applied to the slide surrounding the PTs and a coverslip was mounted onto the nail polish. PTs were imaged with a Leica SP5 laser-scanning confocal microscope, using a UV excitation laser with 405-nm wavelength, a Substrat dichroic beam splitter (Leica, https://www.leica-microsystems.com) and detectors that were set to capture light in the wavelength range of 411–502 nm. Image acquisition and analysis was carried out as described above for immunolocalization.

For the imaging of EXO70A2-mNG fusions, PTs were grown *in vitro* on PGM plates with cellophane for 2 h. After this time, the cellophane was transferred to a slide and a drop of agarose-free PGM with 4 μM FM4-64 was added on top of the cellophane and PTs. Nail polish was applied to the slide and a coverslip was added on top of the nail polish, covering the liquid media. PTs were imaged using a Leica SP5 laser-scanning confocal microscope, 10 min after FM4-64 application. To image EXO70A2-mNG, we used an excitation laser with 488-nm wavelength, a RSP500 dichroic beam splitter and detectors thart were set to capture light with a wavelength range of 494–575 nm. To image FM4-64, we used an excitation laser with 514 nm wavelength, a DD 458/514 dichroic beam splitter, and detectors were set to capture light with a wavelength range of 620–783 nm.

To analyze secretion of the GF(EXT3)P reporter, PTs were grown for 1–2 h under normal *in vitro* conditions on PGM plates with a layer of cellophane. To induce plasmolysis, PTs were transferred to PGM plates containing 25% sucrose (versus 10% for standard plates), without cellophane. Plasmolysis could be observed within a few minutes of transfer. Plasmolyzed PTs expressing GF

(EXT3)P were imaged at 40× magnification using a Leica DM5500 compound microscope. To measure fluorescent signal intensity at the plasmolyzed cell wall region, a region of interest (ROI) was drawn in the entire plasmolyzed region using the differential interference contrast (DIC) channel, excluding the plasma membrane boundary. This ROI was then added to the fluorescent channel and the mean fluorescence intensity was measured. For the cytoplasm measurements, two ROIs of approximately 5 μm^2 were selected about 10–20 μm from the plasma membrane, and the mean fluorescence intensities of each cytoplasmic ROI were averaged. The average of three background measurements was subtracted from both the cell wall and cytoplasm measurements. The secretion index (SI) was calculated as the ratio of cell wall to cytoplasm signal. A minimum of 30 PTs per genotype were measured and statistical significance was determined using the Benjamini–Hochberg false-discovery rate, with FDR = 0.05.

ACKNOWLEDGMENTS

This material is based upon work supported by the National Science Foundation under grant no. IOS-1755482. This work was also supported by the Danish Councils for Strategic and Independent Research (12-125709, 12-131859) and the Copenhagen University Excellence Program for Interdisciplinary Research (CDO2016). We wish to thank Gregg Sobocinski for microscopy assistance and advice.

AUTHOR CONTRIBUTIONS

CAM designed the study, conducted the *frh* mutant screen and wrote the article. SB carried out all immunofluorescence, microscopy and bioinformatic analysis of whole-genome sequences to identify candidate suppressor mutations, functional rescue assays, and performed crosses and PT phenotyping. BLP and SRM generated the 35S::EXT3ssGF(EXT3)P construct and the *rra2/3* double mutant. AD carried out all other cloning and the JIM20 dot blot and Western blots. AB conducted genotyping and genetic co-segregation experiments. All authors edited the article.

CONFLICT OF INTEREST

The authors declare no conflicts of interest.

DATA AVAILABILITY STATEMENT

High-throughput sequence data are available from the National Center for Biotechnology Information (NCBI) Sequence Read Archive (https://www.ncbi.nlm.nih.gov/Traces/study/?) under project accession number PRJNA574113. All other material and data are available upon request from the corresponding author.

SUPPORTING INFORMATION

Additional Supporting Information may be found in the online version of this article.

Figure S1. *frh1* suppresses most, but not all *hpat1/3* pollen tube (PT) phenotypes. (a–c) Differential interference contrast (DIC) images of PT phenotypic classes: (a) a morphologically normal PT typical of the wild type (WT); (b) a ruptured PT; and (c) a 'branched' PT typical of *hpat1/3* mutants. (d) Time course of an *hpat1/3* branching event imaged at 5-min intervals. The white arrow marks the original tip region; the black arrow marks the newly formed tip derived from a subapical portion of the PT. (e) Frequency of *in vitro* pollen germination after 3 h of growth. Pollen were considered germinated if a visible tube of at least one half the length of the pollen grain was identifiable. Note that the reduced germination in *hpat1 hpat3* resultis in part from poor tube elongation. $n > 600$ per genotype. (f) Frequency of PT rupture for the indicated genotypes. No ruptured tubes were observed in WT. $n > 500$ per genotype. (g) Percentage of tubes with two morphologically distinct tip regions after 5 h of *in vitro* PT growth. $n > 200$ per genotype. (h) Average PT widths (±SDs, $n \geq 103$ for each genotype). (i) PT growth rates. Asterisks in (h) and (i) mark statistically significant Student's *t*-test *P* values: $*P \leq 0.05$; $***P \leq 0.0005$.

Figure S2. The JIM20 monoclonal antibody recognizes Hyp-Ara. (a) Illustration of the Hyp-Ara modification and the enzymes responsible for the addition of each arabinose. (b) The EXT antibody JIM20 requires Hyp substituted with at least three arabinoses, i.e. the presence of the HPAT, RRA and XEG113 enzymes, for recognition. Dot blot and SDS-PAGE Western blot analysis of protein isolated from seedlings (top, dot blot) or extracted from rosette leaves (bottom, Western blot) of the indicated genotypes and probed JIM20. (c–e) JIM20 immunostaining visualized with an FITC-conjugated secondary antibody (left) of pollen tubes (PTs, top) and pollen grains (bottom) compared with the corresponding DIC images (right). Images taken at 20× magnification. (c) Wild-type Columbia-0 pollen samples produced robust JIM20 signal in both pollen grains and PTs, particularly near the PT tip. (d) Secondary antibody alone control staining did not produce a detectable signal. (e) In *hpat1/3* pollen samples no JIM20 signal was detected. (f) *frh1 hpat1/3* and *hpat1/3* pollen displayed similar appearance, with no detectable JIM20 signal. All immunolocalizations were imaged using the same light intensity and exposure settings.

Figure S3. Alignment of Arabidopsis EXO70 protein sequences in the region of the exo70a2-2 G319E mutation. CLUSTAL OMEGA multiple sequence alignment of whole protein sequences were trimmed to the region of interest. The EXO70A2 G319 position is hghllighted with red. '*', conserved residues; ':', positions with conservation of amino acids with strongly similar properties; and '.', conservation between weakly similar amino acid properties.

Figure S4. The *exo70a2-2* mutation co-segregates with the *frh1* suppressive phenotype. (a) PCR and restriction enzyme mediated genotyping of 20 *frh1* BC5 F_2 individuals visualized on an agarose gel. The *exo70a2-2* mutation creates a Taqαl restriction enzyme recognition site. The upper band is the un-cut wild-type (WT) product and the lower band is the cleaved *exo70a2-2* product. The two individuals with a non-suppressed phenotype are marked by '*' and both are homozygous WT. (b) Table of the *exo70a2-2* genotype distribution for 123 *frh1* BC5 F_2 plants. The 11 wild-type individuals (+/+) were all non-suppressed, all remaining plants (heterozygous, +/−; homozygous mutant, −/−) were phenotypically suppressed. Note also the significant distortion of genotype ratio compared with the Mendelian 25:50:25% ratio (chi-square test, $P = 2.42 \times 10^{-7}$). This bias against the recovery of homozygous WT plants is consistent with the genetic behavior of *frh1*. (c) Average number of seeds per silique (±SD, $n \geq 16$) in the BC5 F_2 population grouped by *exo70a2-2* genotype. Asterisks mark

statistically significant Student's *t*-test *P* values: $^{**}P \leq 0.005$; $^{***}P \leq 0.0005$.

Figure S5. *frh1* suppression is caused by a mutation in *exo70a2*. (a) *frh1 hpat1/3* plants were transformed with a rescue construct containing the wild-type (WT) genomic EXO70A2 region and seed-expressed fluorescence reporter selection cassette (*OLE1-GFP*; Shimada *et al.*, 2010). Transgene transmission efficiency (TE) for three independent hemizygous single-locus insertion transgenic lines. '**' marks significant difference from the expected TE for no effect of the transgene on transmission (100%, Student's *t*-test $P < 0.005$, $n \geq 185$). (b) Transmission of a control construct containing the strong pollen promoter (Lat52) driving expression of the fluorescent protein mNeonGreen in four independent *frh1 hpat1/3* lines ($n \geq 72$). (c) Seed counts of T_3 plants segregating for the rescue construct. Plants not carrying the rescue construct (0/0) maintained suppressor-levels of seed set. Seed set of plants homozygous for the presence of the rescue construct (+/+) was not statistically different from that of the *hpat1/3* background ($^{***}P < 0.0005$; Student's *t*-test versus *hpat1/3;* $n \geq 15$ siliques).

Figure S6. *exo70a2-2* PTs maintain cell wall polymer polarity in the wild-type (WT) background. (a) Medial *Z*-slices of pollen tubes (PTs) stained with LM19 primary antibody and anti-rat FITC-conjugated secondary antibody, and corresponding quantification of fluorescent signal intensity along the PT periphery, starting at the tip (distance on *x*-axis = 0 μm) to 25 μm down the shaft. (b) Medial *Z*-slices of PTs stained with LM20 primary antibody and anti-rat FITC-conjugated secondary antibody, and corresponding quantification of fluorescent signal intensity as in (a). (c) Maximum projections of PTs stained with aniline blue fluorochrome (ABF) and corresponding quantification of fluorescent signal intensity starting at the tip (distance on *x*-axis = 0) to 50 μm down the shaft of the PT. (d) Medial *Z*-slices of PTs stained with JIM20 primary antibody and anti-rat FITC-conjugated secondary antibody, and corresponding fluorescent signal quantification as in (a) and (b). Colored lines represent means and shading represents standard error. Vertical dashed line represents the approximate region of the PT where the apical dome transitions to the shaft. $n \geq 30$ PTs for each genotype per experiment. All images were acquired by confocal microscopy at 100× magnification. Scale bars: 10 μm.

Figure S7. EXO70A2-mNG rescues pollen tube (PT) germination in the *exo70a2-3* mutant. (a) PTs were grown *in vitro* for 2 h and imaged with a GFP filter (left) and DIC optics (right). Wild-type untransformed Columbia PTs are shown as a negative control for fluorescence. (b) Pollen germination frequency in *exo70a2-3*. The presence of EXO70A2-mNG significantly increased pollen germination compared with the background. The point mutant allele EXO70A2-2 (G319E) also increased pollen germination to a smaller degree. Each point is a datum from a single independent T_1 plant, $n \geq 321$ pollen grains per T_1. $^{***}P < 0.0005$, $^{**}P < 0.005$, $^{*}P < 0.05$. (c) Percentage of fluorescent PTs for *exo70a2-3* EXO70A2-mNG hemizygous lines.

Table S1. Illumina sequencing read information. DNA samples of the indicated genotype, all in the *hpat1/3* background, were sequenced by paired-end Illumina sequencing. At least 97% of reads were aligned to the Columbia reference genome, yielding an estimated genome coverage of between 18- and 63-fold.

Table S2. Full list of sequence variants passing filtering for *frh1*: AO, alternate observations (number of reads with the alternative nucleotide); RO, reference observations (number of reads carrying the reference nucleotide); TO, total observations (AO + RO). Allele frequency is estimated from reads as (AO/TO). Gene functional annotations for those genes with missense mutations are show in black; silent, UTR or intronic mutations are in gray. Double lines are separate chromosomes. The *exo70a2* mutation is in bold.

Table S3. Full list of sequence variants passing filtering for *frh2*: AO, alternate observations (number of reads with the alternative nucleotide); RO, reference observations (number of reads carrying the reference nucleotide); TO, total observations (AO + RO). Allele frequency is estimated from reads as (AO/TO). Gene functional annotations for those genes with missense mutations are show in black; silent, UTR or intronic mutations are in gray. Double lines separate chromosomes. The *sec15a* mutation is in bold.

Table S4. Primers used in this study.

REFERENCES

Adams, E. and Frank, L. (1980) Metabolism of proline and the hydroxyprolines. *Annu Rev Biochem.* **49**, 1005–1061.

Alonso, J.M., Stepanova, A.N., Leisse, T.J. *et al.* (2003) Genome-wide insertional mutagenesis of Arabidopsis thaliana. *Science*, **301**, 653–657.

Bate, N. and Twell, D. (1998) Functional architecture of a late pollen promoter: pollen-specific transcription is developmentally regulated by multiple stage-specific and co-dependent activator elements. *Plant Mol. Biol.* **37**, 859–869.

Beuder, S. and MacAlister, C.A. (2020) Isolation and cloning of suppressor mutants with improved pollen fertility (2020). In: *Pollen and Pollen Tube Biology: Methods and Protocols* (Geitmann, A., ed). MIMB, Humana Press.

Bloch, D., Pleskot, R., Pejchar, P., Potocký, M., Trpkošová, P., Cwiklik, L., Vukašinović, N., Sternberg, H., Yalovsky, S. and Žárský, V. (2016) Exocyst SEC3 and phosphoinositides define sites of exocytosis in pollen tube initiation and growth. *Plant Physiol.* **172**, 980–1002.

Borassi, C., Sede, A.R., Mecchia, M.A., Salter, J.D.S., Marzol, E., Muschietti, J.P. and Estevez, J.M. (2016) An update on cell surface proteins containing extensin-motifs. *J. Exp. Bot.* **67**, 477–487.

Bosch, M. and Hepler, P.K. (2005) Pectin methylesterases and pectin dynamics in pollen tubes. *Plant Cell*, **17**, 3219–3226.

Bove, J., Vaillancourt, B., Kroeger, J., Hepler, P.K., Wiseman, P.W. and Geitmann, A. (2008) Magnitude and direction of vesicle dynamics in growing pollen tubes using spatiotemporal image correlation spectroscopy and fluorescence recovery after photobleaching. *Plant Physiol.* **147**, 1646–1658.

Brownleader, M.D. and Dey, P.M. (1993) Purification of extensin from cell walls of tomato (hybrid of Lycopersicon esculentum and L. peruvianum) cells in suspension culture. *Planta*, **191**, 457–469.

Campanoni, P. and Blatt, M.R. (2007) Membrane trafficking and polar growth in root hairs and pollen tubes. *J. Exp. Bot.* **58**, 65–74.

Cannon, M.C., Terneus, K., Hall, Q., Tan, L., Wang, Y., Wegenhart, B.L., Chen, L., Lamport, D.T.A., Chen, Y. and Kieliszewski, M.J. (2008) Self-assembly of the plant cell wall requires an extensin scaffold. *Proc. Natl. Acad. Sci. USA*, **105**, 2226–2231.

Chang, M. and Huang, S. (2017) Rapid isolation of total protein from *Arabidopsis* pollen. *Bio-Protocol*, **7**(8), e2227. https://doi.org/10.21769/BioProtoc.2227

Chebli, Y., Kaneda, M., Zerzour, R. and Geitmann, A. (2012) The cell wall of the Arabidopsis pollen tube –spatial distribution, recycling, and network formation of polysaccharides. *Plant Physiol.* **160**, 1940–1955.

Chen, Y., Dong, W., Tan, L., Held, M.A. and Kieliszewski, M.J. (2015) Arabinosylation plays a crucial role in extensin cross-linking in vitro. *Biochem. Insights*, **8**, 1–13.

Cheung, A.Y., Niroomand, S., Zou, Y. and Wu, H.-M. (2010) A transmembrane formin nucleates subapical actin assembly and controls tip-focused growth in pollen tubes. *Proc. Natl. Acad. Sci. USA*, **107**, 16390–16395.

Cheung, A.Y. and Wu, H. (2004) Overexpression of an Arabidopsis formin stimulates supernumerary actin cable formation from pollen tube cell membrane. *Plant Cell*, **16**, 257–269.

Chong, Y.T., Gidda, S.K., Sanford, C., Parkinson, J., Mullen, R.T. and Goring, D.R. (2009) Characterization of the Arabidopsis thaliana exocyst complex gene families by phylogenetic, expression profiling, and subcellular localization studies. *New Phytol.* **185**, 401–419.

Choudhary, P., Saha, P., Ray, T., Tang, Y., Yang, D. and Cannon, M.C. (2015) *EXTENSIN18* is required for full male fertility as well as normal vegetative growth in Arabidopsis. *Front. Plant Sci.* **6**, 553.

Cole, R.A., Synek, L., Zarsky, V. and Fowler, J.E. (2005) SEC8, a subunit of the putative Arabidopsis Exocyst complex, facilitates pollen germination and competitive pollen tube growth. *Plant Physiol.* **138**, 2005–2018.

Cole, R.A., McInally, S.A. and Fowler, J.E. (2014) Developmentally distinct activities of the exocyst enable rapid cell elongation and determine meristem size during primary root growth in Arabidopsis. *BMC Plant Biol.* **14**, 386.

Cosgrove, D.J. (2005) Growth of the plant cell wall. *Nat. Rev. Mol. Cell Biol.* **6**, 850–861.

Dardelle, F., Lehner, A., Ramdani, Y., Bardor, M., Lerouge, P., Driouich, A. and Mollet, J.C. (2010) Biochemical and immunocytological characterizations of Arabidopsis pollen tube cell wall. *Plant Physiol.* **153**, 1563–1576.

Egelund, J., Obel, N., Ulvskov, P., Geshi, N., Pauly, M., Bacic, A. and Petersen, B.L. (2007) Molecular characterization of two Arabidopsis thaliana glycosyltransferase mutants, rra1 and rra2, which have a reduced residual arabinose content in a polymer tightly associated with the cellulosic wall residue. *Plant Mol. Biol.* **64**, 439–451.

Everdeen, D.S., Kiefer, S., Willard, J.J., Muldoon, E.P., Dey, P.M., Li, X.B. and Lamport, D.T. (1988) Enzymic cross-linkage of monomeric Extensin precursors in vitro. *Plant Physiol.* **87**, 616–621.

Fabrice, T.N., Vogler, H., Draeger, C., Munglani, G., Gupta, S., Herger, A.G., Knox, P., Grossniklaus, U. and Ringli, C. (2018) LRX proteins play a crucial role in pollen grain and pollen tube cell wall development. *Plant Physiol.* **176**, 1981–1992.

Fry, S.C. (1988) *The Growing Plant Cell Wall: Chemical and Metabolic Analysis*. UK: Longman Scientific & Technical.

Gille, S., Hansel, U., Ziemann, M. and Pauly, M. (2009) Identification of plant cell wall mutants by means of a forward chemical genetic approach using hydrolases. *Proc. Natl. Acad. Sci. USA*, **106**, 14699–14704.

Grobei, M.A., Qeli, E., Brunner, E., Rehrauer, H., Zhang, R., Roschitzki, B., Basler, K., Ahrens, C.H. and Grossniklaus, U. (2009) Deterministic protein inference for shotgun proteomics data provides new insights into Arabidopsis pollen development and function. *Genome Res.* **19**, 1786–1800.

Hála, M., Cole, R., Synek, L. *et al.* (2008) Exocyst complex functions in plant cell growth in Arabidopsis and tobacco. *Plant Cell*, **20**, 1330–1345.

Harsay, E. and Bretscher, A. (1995) Parallel secretory pathways to the cell surface in yeast. *J. Cell Biol.* **131**, 297–310.

He, B., Xi, F., Zhang, X., Zhang, J. and Guo, W. (2007a) Exo70 interacts with phospholipids and mediates the targeting of the exocyst to the plasma membrane. *EMBO J.* **26**, 4053–4065.

He, B., Xi, F., Zhang, J., TerBush, D., Zhang, X. and Guo, W. (2007b) Exo70p mediates the secretion of specific exocytic vesicles at early stages of the cell cycle for polarized cell growth. *J. Cell Biol.* **176**, 771–777.

Held, M.A., Tan, L., Kamyab, A., Hare, M., Shpak, E. and Kieliszewski, M.J. (2004) Di-isodityrosine is the intermolecular cross-link of isodityrosine-rich extensin analogs cross-linked in vitro. *J. Biol. Chem.* **279**, 55474–55482.

Hepler, P.K., Rounds, C.M. and Winship, L.J. (2013) Control of cell wall extensibility during pollen tube growth. *Mol. Plant*, **6**, 998–1017.

Hill, A.E., Shachar-Hill, B., Skepper, J.N., Powerll, A. and Shachar-Hill, Y. (2012) An osmotic model of the growing pollen tube. *PLoS ONE*, **7**, e36585.

Hruz, T., Laule, O., Szabo, G., Wessendorp, F., Bleuler, S., Oertle, L., Widmayer, P., Gruissem, W. and Zimmermann, P. (2008) Genevestigator v3: a reference expression database for the meta-analysis of transcriptomes. *Adv. Bioinform.* **2008**, 420747.

Imin, N., Patel, N., Corcilius, L., Payne, R.J. and Djordjevic, M.A. (2018) CLE peptide tri-arabinosylation and peptide domain sequence composition are essential for SUNN-dependent autoregulation of nodulation in Medicago truncatula. *New Phytol.* **218**, 73–80.

Johnson, K.L., Cassin, A.M., Lonsdale, A., Bacic, A., Doblin, M.S. and Schultz, C.J. (2017) Pipeline to identify hydroxyproline-rich glycoproteins. *Plant Physiol.* **174**, 886–903.

Kalmbach, L., Hématy, K., De Bellis, D., Barberon, M., Fujita, S., Ursache, R., Daraspe, J. and Geldner, N. (2017) Transient cell-specific EXO70A1 activity in the CASP domain and Casparian strip localization. *Nat. Plants*, **3**, 17058.

Kanaoka, M.M. and Higashiyama, T. (2015) Peptide signaling in pollen tube guidance. *Curr. Opin. Plant Biol.* **28**, 127–136.

Kassaw, T., Nowak, S., Schnabel, E. and Frugoli, J. (2017) ROOT DETERMINED NODULATION1 is required for M. truncatula CLE12, but not CLE13, peptide signaling through the SUNN receptor kinase. *Plant Physiol.* **174**, 2445–2456.

Kieliszewski, M.J. and Shpak, E. (2001) Synthetic genes for the elucidation of glycosylation codes for arabinogalactan-proteins and other hydroxyproline-rich glycoproteins. *Cell. Mol. Life Sci.* **58**, 1386–1398.

Klepikova, A.V., Kasianov, A.S., Gerasimov, E.S., Logacheva, M.D. and Penin, A.A. (2016) A high resolution map of the Arabidopsis thaliana developmental transcriptome based on RNA-seq profiling. *Plant J.* **88**, 1058–1070.

Kulich, I., Cole, R., Drdová, E., Cvrčková, F., Soukup, A., Fowler, J. and Žárský, V. (2010) Arabidopsis exocyst subunits SEC8 and EXO70A1 and exocyst interactor ROH1 are involved in the localized deposition of seed coat pectin. *New Phytol.* **188**, 615–625.

Lamport, D.T.A. and Miller, D.H. (1971) Hydroxyproline Arabinosides in the Plant Kingdom. *Plant Physiol.* **48**, 454–456.

Lamport, D.T.A. (1967) Hydroxyproline-O-glycosidic linkage of the plant cell wall glycoprotein extensin. *Nature*, **216**, 1322–1324.

Leucci, M.R., Sansebastiano, P.D., Gigante, M., Dalessandro, G. and Piro, G. (2007) Secretion marker proteins and cell-wall polysaccharides move through different secretory pathways. *Planta*, **225**, 1001–1017.

Li, Y., Tan, X., Wang, M., Li, B., Zhao, Y., Wu, C. and Rui, Q. (2017) Exocyst subunit SEC3A marks the germination site and is essential for pollen germination in Arabidopsis thaliana. *Sci Rep.* **7**, 40279.

Li, S., Chen, M., Yu, D., Ren, S., Sun, S., Liu, L., Ketelaar, T., Emons, A.M. and Liu, C.M. (2013) EXO70A1-mediated vesicle trafficking is critical for tracheary element development in Arabidopsis. *Plant Cell*, **25**, 1774–1786.

Li, S., van Os, G.M., Ren, S., Yu, D., Ketelaar, T., Emons, A.M. and Liu, C.M. (2010) Expression and functional analyses of EXO70 genes in Arabidopsis implicate their roles in regulating cell type-specific exocytosis. *Plant Physiol.* **154**, 1819–1830.

Liu, J., Zuo, X., Yue, P. and Guo, W. (2007) Phosphatidylinositol 4,5-bisphosphate mediates the targeting of the exocyst to the plasma membrane for exocytosis in mammalian cells. *Mol. Biol. Cell*, **18**, 4483–4492.

MacAlister, C.A., Ortiz-Ramírez, C., Becker, J.D., Feijó, J.A. and Lippman, Z.B. (2016) Hydroxyproline O-arabinosyltransferase mutants oppositely alter tip growth in Arabidopsis thaliana and Physcomitrella patens. *Plant J.* **85**, 193–208.

Marković, V., Cvrčková, F., Potocký, M., Pejchar, P., Kollárová, E., Kulich, I., Synek, L. and Žárský, V. (2019) EXO70A2 is critical for the exocyst complex function in Arabidopsis pollen. *bioRxiv*. https://doi.org/10.1101/831875

McKenna, S.T., Kunkel, J.G., Bosch, M., Rounds, C.M., Vidali, L., Winship, L.J. and Hepler, P.K. (2009) Exocytosis precedes and predicts the increase in growth in oscillating pollen tubes. *Plant Cell*, **21**, 3026–3040.

Mecchia, M.A., Santos-Fernandez, G., Duss, N.N. *et al.* (2017) RALF4/19 peptides interact with LRX proteins to control pollen tube growth in Arabidopsis. *Science*, **358**(6370), 1600–1603.

Micheli, F. (2001) Pectin methylesterases: cell wall enzymes with important roles in plant physiology. *Trends Plant Sci.* **6**, 414–419.

Mei, K. and Guo, W. (2018) The exocyst complex. *Curr. Biol.* **28**, R922–R925.

Møller, S.R., Yi, X., Velásquez, S.M. *et al.* (2017) Identification and evolution of a plant cell wall specific glycoprotein glycosyl transferase. *ExAD. Scientific Reports*, **7**, 45341.

Ogawa-Ohnishi, M., Matsushita, W. and Matsubayashi, Y. (2013) Identification of three hydroxyproline O-arabinosyltransferases in Arabidopsis thaliana. *Nat. Chem. Biol.* **9**, 726–730.

Ohyama, K., Shinohara, H., Ogawa-Ohnishi, M. and Matsubayashi, Y. (2009) A glycopeptide regulating stem cell fate in Arabidopsis thaliana. *Nat. Chem. Biol.* **5**, 578–580.

Peterson, R., Sloven, J.P. and Chen, C. (2010) A simplified method for differential staining of aborted and non-aborted pollen grains. *Int. J. Plant Biol.* **1**, e13.

Qi, X., Behrens, B.X., West, P.R. and Mort, A.J. (1995) Solubilization and partial characterization of extensin fragments from cell walls of cotton suspension cultures. Evidence for a covalent cross-link between extensin and pectin. *Plant Physiol.* **108**, 1691–1701.

Rodriguez-Enriquez, M.J., Mehdi, S., Dickinson, H.G. and Grant-Downton, R.T. (2013) A novel method for efficient in vitro germination and tube growth of Arabidopsis thaliana pollen. *New Phytol.* **197**, 668–679.

Rounds, C.M., Lubeck, E., Hepler, P.K. and Winship, L.J. (2011) Propidium iodide competes with Ca(2+) to label pectin in pollen tubes and Arabidopsis root hairs. *Plant Physiol.* **157**, 175–187.

Safavian, D., Zayed, Y., Indriolo, E., Chapman, L., Ahmed, A. and Goring, D. (2015) RNA silencing of exocyst genes in the stigma impairs the acceptance of compatible pollen in Arabidopsis. *Plant Physiol.* **169**, 2526–2538.

Samuel, M.A., Chong, Y.T., Haasen, K.E., Aldea-Brydges, M.G., Stone, S.L. and Goring, D.R. (2009) Cellular pathways regulating responses to compatible and self-incompatible pollen in Brassica and Arabidopsis stigmas intersect at Exo70A1, a putative component of the Exocyst complex. *Plant Cell*, **21**, 2655–2671.

Schlupmann, H., Bacic, A. and Read, S.M. (1994) Uridine diphosphate glucose metabolism and callose synthesis in cultured pollen tubes of Nicotiana alata Link et Otto. *Plant Physiol.* **105**(2), 659–670.

Schnabel, E.L., Kassaw, T.K., Smith, L.S., Marsh, J.F., Oldroyd, G.E., Long, S.R. and Frugoli, J.A. (2011) The ROOT DETERMINED NODULATION1 gene regulates nodule number in roots of Medicago truncatula and defines a highly conserved, uncharacterized plant gene family. *Plant Physiol.* **157**, 328–340.

Sede, A.R., Borassi, C., Wengier, D.L., Mecchia, M.A., Estevez, J.M. and Muschietti, J.P. (2018) Arabidopsis pollen extensins LRX are required for cell wall integrity during pollen tube growth. *FEBS Letters*, **592**, 233–243.

Sekereš, J., Pejchar, P., Šantrůček, J., Vukašinović, N., Žárský, V. and Potocký, M. (2017) Analysis of Exocyst subunit EXO70 family reveals distinct membrane polar domains in tobacco pollen tubes. *Plant Physiol.* **173**, 1659–1675.

Shaner, N.C., Lambert, G.G., Chammas, A. *et al.* (2013) A bright monomeric green fluorescent protein derived from Branchiostoma lanceolatum. *Nat. Methods*, **10**, 407–409.

Shimada, T.L., Shimada, T. and Hara-Nishimura, I. (2010) A rapid and non-destructive screenable marker, FAST, for identifying transformed seeds of Arabidopsis thaliana. *Plant J.* **61**, 519–528.

Showalter, A.M., Keppler, B., Lichtenberg, J., Gu, D. and Welch, L.R. (2010) A bioinformatics approach to the identification, classification, and analysis of hydroxyproline-rich glycoproteins. *Plant Physiol.* **153**, 485–513.

Showalter, A.M. and Basu, D. (2016) Extensin and arabinogalactan-protein biosynthesis: glycosyltransferases, research challenges, and biosensors. *Front. Plant Sci.* **7**, 814.

Sinclair, R., Rosquete, M.R. and Drakakaki, G. (2018) Post-Golgi trafficking and transport of cell wall components. *Front. Plant Sci.* **9**, 1784.

Smallwood, M., Martin, H. and Knox, J.P. (1995) An epitope of rice threonine- and hydroxyproline-rich glycoprotein is common to cell wall and hydrophobic plasma-membrane glycoproteins. *Planta*, **196**, 510–522.

Smallwood, M., Beven, A., Donovan, N., Neill, S.J., Peart, J., Roberts, K. and Knox, J.P. (1994) Localization of cell wall proteins in relation to the developmental anatomy of the carrot root apex. *Plant J.* **5**, 237–246.

Stafstrom, J. and Staehelin, L.A. (1986a) Cross-linking patterns in salt-extractable extensin from Carrot cell walls. *Plant Physiol.* **81**, 234–241.

Stafstrom, J.P. and Staehelin, L.A. (1986b) The role of carbohydrate in maintaining extensin in an extended conformation. *Plant Physiol.* **81**, 242–246.

Synek, L., Schlager, N., Eliáš, M., Quentin, M., Hauser, M.T. and Žárský, V. (2006) AtEXO70A1, a member of a family of putative exocyst subunits specifically expanded in land plants, is important for polar growth and plant development. *Plant J.* **48**, 54–72.

Synek, L., Vukašinović, N., Kulich, I., Hála, M., Aldorfová, K., Fendrych, M. and Žárský, V. (2017) EXO70C2 is a key regulatory factor for optimal tip growth of pollen. *Plant Physiol.* **174**, 223–240.

Tan, L., Varnai, P., Lamport, D.T.A., Yuan, C., Xu, J., Qiu, F. and Kieliszewski, M.J. (2010) Plant O-Hydroxyproline arabinogalactans are composed of repeating trigalactosyl subunits with short bifurcated side chains. *J. Biol. Chem.* **285**, 24575–24583.

Tang, H., Wang, S., Wang, J., Song, M., Xu, M., Zhang, M., Shen, Y., Hou, J. and Bao, X. (2016) N-hypermannose glycosylation disruption enhances recombinant protein production by regulating secretory pathway and cell wall integrity in Saccharomyces cerevisiae. *Scientific Reports*, **6**, 25654.

Van der Woude, W.J., Morré, D.J. and Bracker, C.E. (1971) Isolation and characterization of secretory vesicles in germinated pollen of Lilium longiflorum. *J. Cell Sci.* **8**, 331–351.

van Holst, G.J. and Varner, J.E. (1984) Reinforced polyproline II conformation in a hydroxyproline-rich cell wall glycoprotein from carrot root. *Plant Physiol.* **74**, 247–251.

Velasquez, S.M., Marzol, E., Borassi, C. *et al.* (2015) Low sugar is not always good: impact of specific O-glycan defects on tip growth in Arabidopsis. *Plant Physiol.* **168**, 808–813.

Velasquez, S.M., Ricardi, M.M., Dorosz, J.G. *et al.* (2011) O-glycosylated cell wall proteins are essential in root hair growth. *Science*, **332**, 1401–1403.

Verhertbruggen, Y., Marcus, S.E., Haeger, A., Ordaz-Ortiz, J.J. and Knox, J.P. (2009) An extended set of monoclonal antibodies to pectic homogalacturonan. *Carbohyd. Res.* **344**, 1858–1862.

Wang, X., Wang, K., Yin, G. *et al.* (2018) Pollen-expressed leucine-rich repeat extensins are essential for pollen germination and growth. *Plant Physiol.* **176**, 1993–2006.

Wolf, S., Mouille, G. and Pelloux, J. (2009) Homogalacturonan methyl-esterification and plant development. *Mol. Plant*, **2**(5), 851–860.

Woody, S.T., Austin-Phillips, S., Amasino, R.M. and Krysan, P.J. (2007) The WiscDsLox T-DNA collection: an Arabidopsis community resource generated by using an improved high-throughput T-DNA sequencing pipeline. *J. Plant Res.* **120**, 157–165.

Xiang, Y., Zhang, X., Nix, D.B., Katoh, T., Aoki, K., Tiemeyer, M. and Wang, Y. (2012) Regulation of protein glycosylation and sorting by the Golgi matrix proteins GRASP55/65. *Nat. Commun.* **4**, 1659.

Xu, C., Liberatore, K.L., MacAlister, C.A. *et al.* (2015) A cascade of arabinosyltransferases controls shoot meristem size in tomato. *Nat. Genet.* **47**, 784–792.

Yang, Z., Bennett, E.P., Jørgensen, B., Drew, D.P., Arigi, E., Mandel, U., Ulvskov, P., Levery, S.B., Clausen, H. and Petersen, B.L. (2012) Toward stable genetic engineering of human O-glycosylation in plants. *Plant Physiol.* **160**, 450–463.

Ye, J., Zheng, Y., Yan, A., Chen, N., Wang, Z., Huang, S. and Yang, Z. (2009) Arabidopsis formin3 directs the formation of actin cables and polarized growth in pollen tubes. *Plant Cell*, **21**, 3868–3884.

Yoro, E., Nishida, H., Ogawa-Ohnishi, M., Yoshida, C., Suzaki, T., Matsubayashi, Y. and Kawaguchi, M. (2019) PLENTY, a hydroxyproline O-arabinosyltransferase, negatively regulates root nodule symbiosis in Lotus japonicus. *J. Exp. Bot.* **70**, 507–517.

Zhu, X., Li, S., Pan, S., Xin, X. and Gua, Y. (2018) CSI1, PATROL1, and exocyst complex cooperate in delivery of cellulose synthase complexes to the plasma membrane. *Proc. Natl. Acad. Sci. USA*, **115**, E3578–E3587.